




Pulsating linear in situ combustion: why do we often observe oscillatory behavior?

Mohammad Bazargan¹ · Anthony R. Kovscek¹ 

Received: 4 May 2017 / Accepted: 27 March 2018 / Published online: 9 May 2018
© Springer International Publishing AG, part of Springer Nature 2018

Abstract

We have studied simplified, pulsating, one-dimensional, in situ combustion processes. For two cases, with different reaction stoichiometry, oscillations in temperature, flue gas rate, and flue gas composition are demonstrated and the parameter space resulting in oscillatory behavior is identified. To understand the role of different parameters, linear stability of the problem is studied. Because linear stability analysis requires the solution of uniform front propagation, we investigated an asymptotic analytical solution of the problem. We found an original formula for the front propagation velocity. The analytical solution enabled us to define four dimensionless parameters including Zeldovich (Ze) number, Damkohler (Da) number, a specialized air-fuel ratio (B), and a ratio incorporating air and rock heat capacities (Δ_1). Using linear stability analysis, we show that the stability of the problem is also governed by these four parameters. Because $\Delta_1 \approx 1$ for typical laboratory conditions, the set of (Ze , Da , B) is used to construct the stability plane; consequently, several important design considerations are suggested. Both larger air injection rate and air enriched in oxygen increase the front propagation speed but push the system toward oscillatory behavior. Conversely, the introduction of catalysts and metal additives, that decrease the activation energy of reactions, increases the front speed and stability. Similarly, increasing the amount of fuel available for the combustion makes the design more stable and drives the combustion front to propagate more quickly.

Keywords In situ combustion · Combustion tube experiment · Oscillation · Pulsating combustion · Smoldering combustion · Stability analysis

1 Introduction

In situ combustion (ISC) is an enhanced oil recovery (EOR) method. During ISC, air is injected into the reservoir to burn part of the crude-oil and produce heat and combustion gases. Heat considerably reduces the oil viscosity and combustion gases push the oil toward the producer [43]. ISC has been successfully applied in the field [41]. Nevertheless, ISC design and prediction is one of the most challenging problems in petroleum engineering [21, 28]. Complex oil

oxidation kinetics in porous media [13] are combined with mass and heat transfer phenomena.

Conventionally, there are two laboratory experiments to help the design ISC at the field-scale. Kinetics cell (KC) experiments [15] are designed to focus on the kinetics of crude-oil oxidation and remove the complexity caused by the flow of liquid phases. Combustion tube (CT) experiments are ISC in one-dimension [44]. Some researchers have suggested that results of combustion tube tests are a clear indication of the likelihood of successful ISC in the field [39]. Numerical simulations are typically constructed to match combustion tube results [29]. Ideally, if the simulation matched the combustion tube results, the model can be used for field scale simulation for given geological conditions. There are two major problems, however. First, direct application of Arrhenius-based kinetics models at the field scale is challenging [54]. Second, to date, there has not been a model for a

✉ Mohammad Bazargan
mozarg@stanford.edu

Anthony R. Kovscek
kovscek@stanford.edu

¹ Energy Resources Engineering Department, Stanford University, 367 Panama St, Stanford CA, 94305-2220, USA

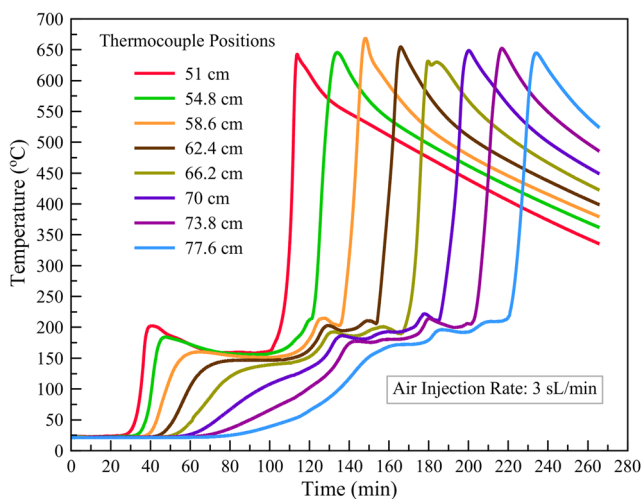


Fig. 1 Temperature profile for a CT experiment of a crude-oil sample [11]

given crude-oil that predicts CT experiments at different conditions (see the model used by [32]). There seems to be a lack of full understanding of the dynamics of the in situ combustion process even at the lab scale.

Observations from CT experiments, are that the flue gas composition profiles, often show oscillatory behavior. Figures 1 and 2 depict our experimental CT results for one crude-oil sample. Figure 1 shows the temperature history recorded at various thermocouples along the length of the CT and Fig. 2 shows O_2 and CO_2 composition of the flue gas versus time. We see that the flue gas composition oscillates significantly while the peak temperature slightly oscillates between 640 and 660 °C.

Results of several CT experiments have been analyzed using X-ray imaging [22, 23]. Similar oscillatory behavior

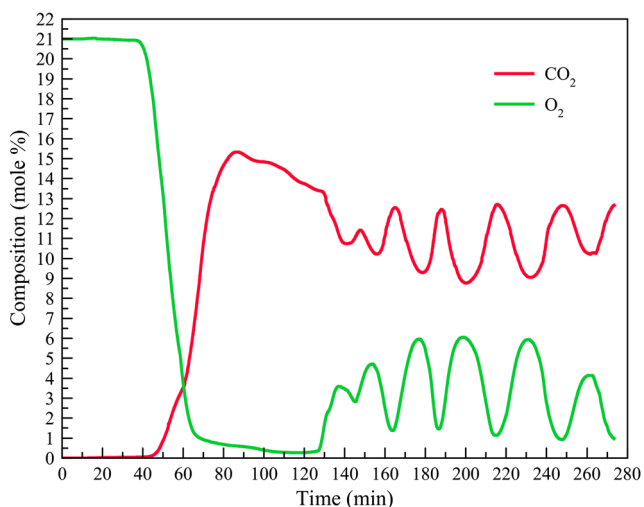


Fig. 2 Flue gases composition histories for a CT experiment of a crude-oil sample [11]

was observed. [22] suggested that the oscillations in the gas composition profile correlate with the peak temperature variation of the temperature profile. Yet, no explanation was given for these oscillatory profiles.

Oscillatory behavior, referred to as pulsation, is very well studied in the context of solid fuel combustion, both experimentally and analytically. Reference [47] seems to be the first to study pulsating behavior of gasless combustion. That is, combustion of the condensed phase in porous media without convective flow of oxidizer [36]. Similarly, reference [37] were the first to describe this pulsating behavior using linear stability analysis. They showed that the oscillatory state arises as a time-periodic bifurcation from the uniformly propagating state, when the bifurcation parameter exceeds a critical value (Hopf bifurcation). They used an asymptotic approach to approximate uniform propagation in the linear stability analysis. The Zel'dovich concept [52] was used to describe the pulsating behavior of gasless combustion. For stability analysis of gasless combustion, [46] used the method of matched asymptotic expansion. He concluded that a Zeldovich number of 6 is the critical stability limit for gasless combustion. The same conclusion was made by [20]. There are numerous studies on the stability of gasless combustion, including one dimensional [19], two dimensional [35], spinning behavior in three dimensional case [25], and heat-loss effect [18] studies.

Pulsating behavior is observed in other types of solid fuel combustion. Numerous experimental studies confirm the existence of a pulsating regime of filtration combustion (e.g., [17, 27]). Forced forward smoldering combustion is studied by [45] and [5]. The stability was studied for this type of filtration combustion by many researchers [7, 30]. [51] summarizes the stability results of this type of filtration combustion.

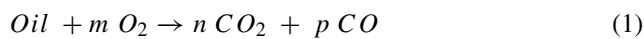
In our paper, we study the pulsating behavior of ISC. In this study, “stability” corresponds to the uniform propagation of the front and is used to contrast with pulsating behavior that is represented by bounded oscillations in measurable quantities.

We begin with the simulation of a simplified CT model of ISC (i.e., convectively dominated heat and mass transfer) to investigate the existence of the pulsating regime. Even though a full analytical treatment of ISC is not possible, we formulate our problem and solve it analytically for uniform propagation of the front. The analytical solution enlightens us to define relevant non-dimensional parameters influencing the dynamics of ISC. Additionally, by linear stability analysis, we show that our non-dimensional parameters are also relevant to describe the stability of the problem. We suggest a stability plane composed of three non-dimensional parameters. In Section 4, we summarize several design considerations based on our findings from stability analysis.

2 Simulation study

We have constructed a simplified ISC model using CMG, [48]. A 3-m long combustion tube is considered to allow sufficient time to study the front propagation and effluent gases. The tube is packed with sand containing oil with a concentration of C_0 . The porosity is 0.36 and is constant. The permeability is 10 Darcy and the pressure drop is negligible. The initial pressure is 780 KPa. Oil is assumed to be in the liquid phase, but below the residual saturation. The water inside the tube is assumed to be negligible. The water component is also removed from the oxidation kinetics of the oil. So, we have two phases of oil and gas with the gas phase as the only moving phase. For the initial ignition, the first 0.3 cm of the tube is heated to reach instantly the temperature of 600 °C and remains constant at this temperature for 15 min. Then, the heater is turned off. Air is injected with the constant mass rate of \dot{m}_{inj} and the oxygen mass fraction of y_{inj} .

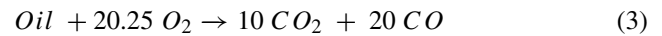
A one-step reaction is considered to represent the global oxidation kinetics of the oil. The reaction is not suitable to represent fully the oil oxidation [10]. In future work, the effect of complex oxidation kinetics of the oil will be investigated (see Section 5). Nevertheless, it is a good first step to understand the dynamics of ISC. We consider:



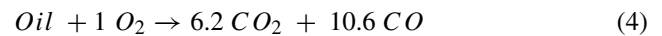
with m , n , and p being the stoichiometric coefficients of O_2 , CO_2 , and CO , respectively. We assume that the reaction rate (\dot{R}) follows the Arrhenius law:

$$\dot{R} = aP y_{O_2} C e^{-\frac{E}{RT}} \tag{2}$$

in which a is the frequency factor, E is the activation energy and P is the pressure. The reaction order with respect to both oil and oxygen are considered to be 1 [13, 49]. Two cases with different stoichiometry are considered (Table 1). In case 1, the stoichiometry is:



For this case, the amount of oxygen consumed to oxidize 1 gr of oil, is 1.27. This ratio (referred to as σ) is normally about 1, for oil oxidation [51]. Nevertheless, to see the effect of σ on the results, this ratio is considered to be 0.06 for case 2. For case 2, the reaction stoichiometry is:



The heat of reaction for both cases is 2.50×10^7 J/(grmole of oil). Other parameters are listed in Table 1.

Figures 3 and 4 show the flue gas molar composition for case 1, and case 2, respectively. We see that after passing the transient time, gas compositions reach constant values. The same conclusion holds for temperature profiles. Figures 5 and 6 demonstrate the temperature profiles at different times for case 1, and case 2, respectively. After the transition period, we see a uniform propagation of the front. This is contradictory to [34] who conclude that partial oxidation causes the oscillatory behavior. Both case 1 and case 2 yield partial oxidation, but they show stable propagation of the front.

We decrease the heat of reaction for both case 1 and case 2. Tables 2 and 3 show the heat of reaction for different scenarios. In Table 2, case 1 is referred to as case 1.1 and other scenarios are referred to as cases 1.2, 1.3, 1.4, and 1.5. Similarly, cases 2.1, 2.2, 2.3, 2.4, and 2.5 are defined.

Table 1 Simulation parameters for case 1 and 2

Parameters	Definition	Unit	Case 1	Case 2
M_{oil}	Molecular Weight of Oil	gr/mol	512	537.6
\dot{m}_{inj}	Injection Mass Rate	gr/min	3.64	2.43
y_{inj}	Oxygen Mass Fraction of the Injected Gas		0.23	0.23
C_0	Initial Oil Concentration	gr/cm ³ of the Bulk Volume	0.03	0.05
ϕ	Porosity		0.36	0.36
K	Permeability	Darcy	10	10
A	Combustion Tube Cross-section	cm ²	100	100
E	Activation Energy	J/mol	120000	125311
a	Frequency Factor	1/psi/min	56208187	56208187
P	Pressure	kPa	780	780
σ	Mass of Oxygen Consumed per Mass of oil Burned		0.06	1.27
c_s	Sand Heat Capacity	J/°C/gr	2.02	2.02
c_p	Gas Heat Capacity	J/°C/gr	1.0467	1.0467
λ	Heat Conductivity of Sand	J/°C/min/cm	1.9	1.9
T_i	Initial Temperature	°C	50	25

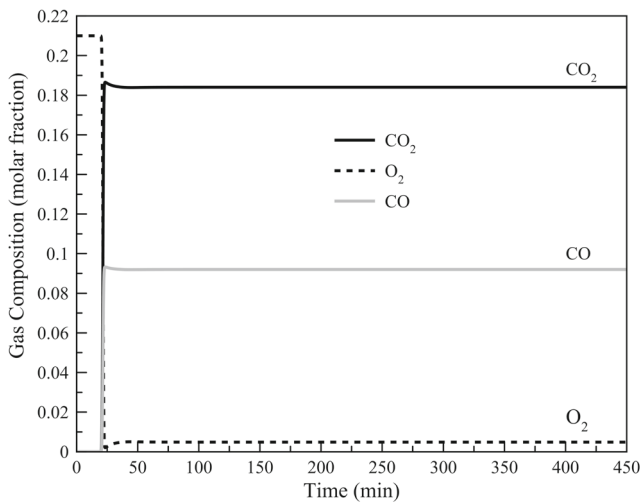


Fig. 3 Effluent gases composition histories for case 1

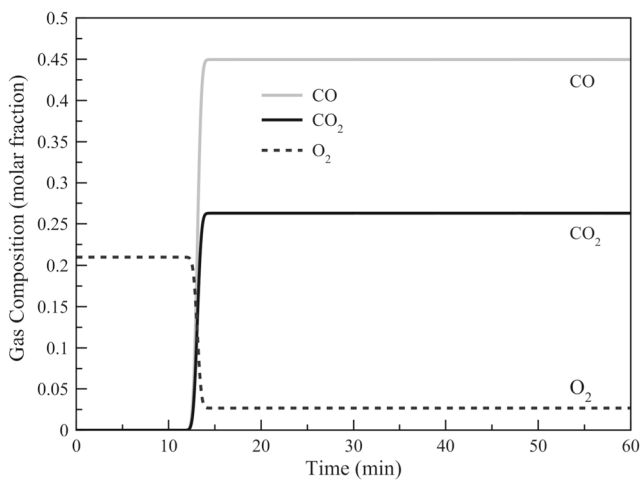


Fig. 4 Effluent gases composition histories for case 2

Table 2 Heat of reaction for different scenarios of case 1

Case 1	Heat of Reaction J/grmole of oil
1.1	2.50×10^7
1.2	2.10×10^7
1.3	1.99×10^7
1.4	1.95×10^7
1.5	1.90×10^7

Table 3 Heat of reaction for different scenarios of case 2

Case	Heat of Reaction J/grmole of oil
2.1	2.50×10^7
2.2	2.20×10^7
2.3	2.15×10^7
2.4	2.10×10^7
2.5	2.00×10^7

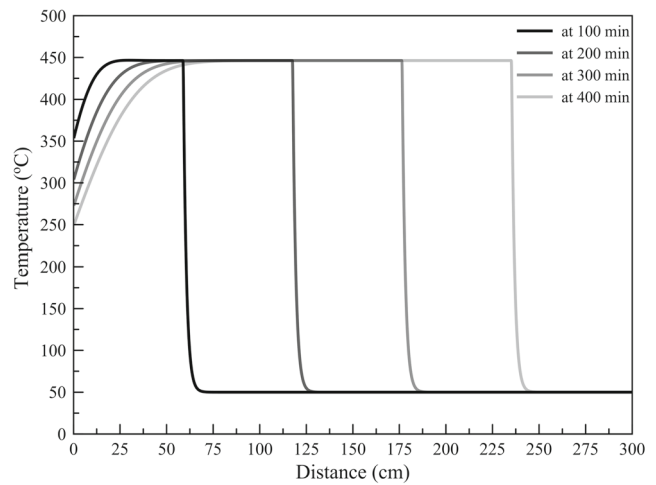


Fig. 5 Temperature profile at different times for case 1

In Appendix 7.3, we show the robustness of our numerical simulation for both stable and pulsating modes. Convergence is achieved by spatial and temporal refinement. Also, we show that our numerical simulation is stable against both infinitesimal and finite perturbations.

Figure 7 shows the molar composition of the oxygen in the flue gases, for different scenarios of case 1. Complete results for flue gas rate, composition and temperature profiles are shown in Appendix 7.4. We see that as the heat of reaction decreases, an oscillation appears in the flue gas composition histories. In case 1.2, the oscillation damps as the propagation continues. As the heat of reaction decreases, the oscillation becomes more severe. The same conclusion is correct for case 2 (Fig. 8). In case 2.2, we see that the oscillation damps as the propagation of the front continues. In case 2.5, we see the oscillatory behavior of the combustion front approaches complete pulsation. Although both case 1 and 2 show the same trend, they exhibit

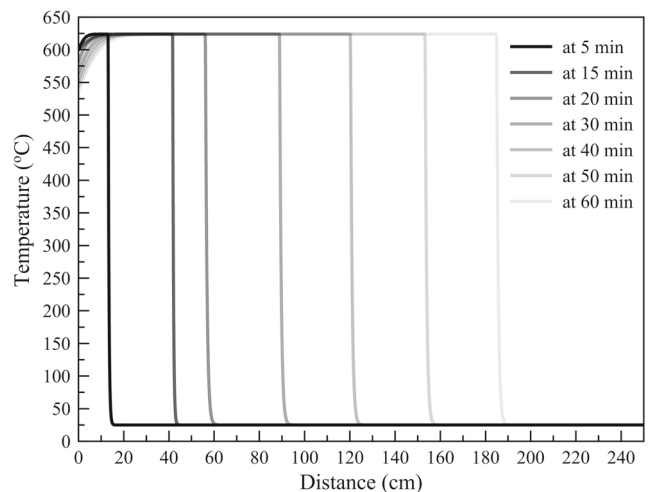


Fig. 6 Temperature profile at different times for case 2

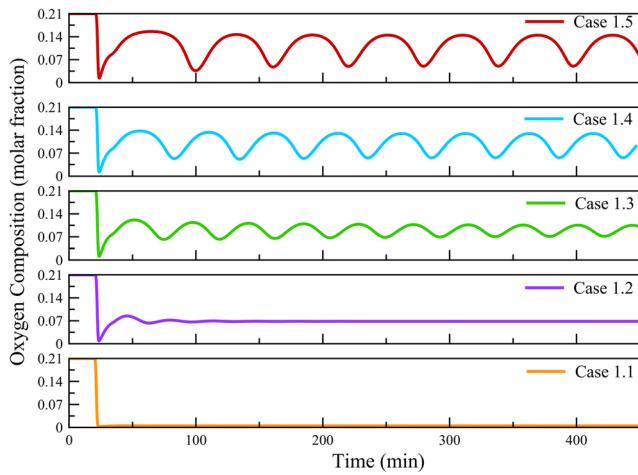


Fig. 7 Effluent molar oxygen composition for different scenarios of case 1. The heat of reaction decreases from top to bottom

different shape of oscillations. We see from figures shown in Appendix 7.4 that the relative amplitude of oscillation is larger in the flue gas rates and composition profiles compared to the temperature profiles. Next, we analyze these pulsating behaviors through a stability analysis of the problem.

3 Scaling analysis

Our objective in this section is to find a set of non-dimensional parameters that governs the dynamics of ISC and characterizes its pulsating behavior. For this purpose, we start by finding the analytical solution for the uniform propagation of the front. We show that the uniform propagation of the front is approximately defined with four non-dimensional parameters. The non-dimensional

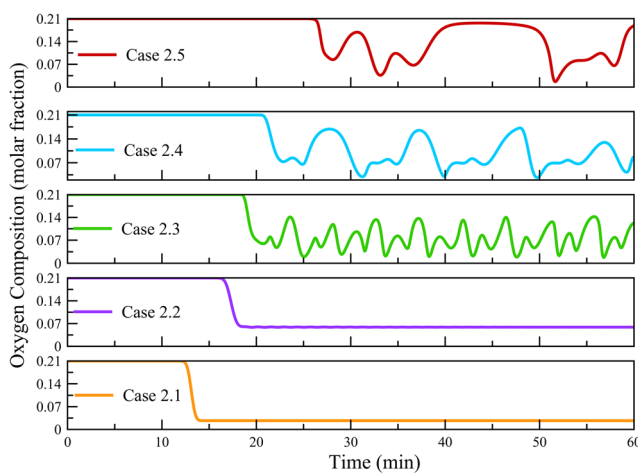


Fig. 8 Effluent molar oxygen composition for different scenarios of case 2. The heat of reaction decreases from top to bottom

parameters used in the analytical approximation of the uniform front propagation may not be sufficient to explain the stability of ISC. Thus, we formulate a linear stability analysis to assess the capability of these parameters to predict the pulsating behavior of ISC.

3.1 Problem formulation

We start by writing the mass balance equations for components in each phase. The gas phase contains four components N_2 , O_2 , CO_2 , and CO . All components are assumed to be non-condensable. In our problem, the accumulation terms in the mass balance equations of the gas phase components are negligible [6]. For the oxygen component, we have:

$$\frac{\partial(\dot{m} y)}{\partial x} + \sigma A \dot{R} = 0$$

in which \dot{m} is the gas mass flow-rate, y is the mass fraction of the oxygen component, σ is the mass of oxygen consumed per mass of oil burned, A is the cross-sectional area of the combustion tube, and \dot{R} is the reaction rate defined by Eq. 2. By adding the equations for each component, we obtain the mass balance equation of the gas phase.

$$\frac{\partial \dot{m}}{\partial x} - A \dot{R} = 0$$

Because the oil is assumed to be non-volatile and its saturation is below residual, we have only the accumulation and reaction terms for the mass balance equation of the oil phase:

$$\frac{\partial C}{\partial t} = -\dot{R}$$

in which C is the concentration of the oil phase defined as the mass of oil per cm^3 of the bulk volume.

The energy balance is written as:

$$\lambda A \frac{\partial^2 T}{\partial x^2} + Q \dot{R} A = \dot{m} c_p \frac{\partial T}{\partial x} + A c_s \frac{\partial T}{\partial t}$$

and in general as:

$$\lambda A \frac{\partial^2 T}{\partial x^2} + Q \dot{R} A = \frac{\partial(\dot{m} H)}{\partial x} + A c_s \frac{\partial T}{\partial t} \tag{5}$$

in which, λ is the thermal conductivity of the rock, Q is the heat of reaction per gram-mole of the oil, H is the enthalpy of the gas phase, c_p is the gas heat capacity, and c_s is volumetric heat capacity of the rock. Because the amount of oil is small, the role of oil-phase heat capacity on the energy balance is small.

3.2 Analytical approach

Stability analysis requires the solution for the uniform propagation of the front. Because we must find the stability limit numerically (see Section 3.4), we do not need to have the full analytical equations for the uniform propagation of the front; however, to define relevant dimensionless numbers (Section 3.3), we must have an analytical expression for the velocity of uniform front propagation.

There have been few analytical studies of ISC [1, 2, 34]. Their approaches are based on the Zeldovich concept [52] that has been implemented in filtration combustion. Like many other combustion problems, non-linearity in filtration combustion is handled using an asymptotic approach [14]. References [8] and [50] approximated the reaction zone to be a plane that is propagating inside the porous medium. Reference [45] used a parameter expansion asymptotic method for smoldering combustion. The work of [3] is based on asymptotic method developed by [45].

The reaction plane approximation of [4] is suitable for our purpose except that the Zeldovich-Frank-Kamenetskii (ZFK) [26] approximation is used for the velocity of the combustion front. This approximation, that is obtained for gasless combustion, is not suitable for our problem that involves the convective terms of gas phase flow. Additionally, [5] solved the problem when the oxygen reaction order is non-zero, by averaging. This approach also needs to be modified.

Considering the reaction front as a plane that propagates with constant velocity inside the porous medium (Fig. 9), we define $\xi = Vx - t$ and $\theta = t$ in which V is the front velocity. The mass and energy balance equations become:

$$\frac{\partial \dot{m}}{\partial \xi} - A \dot{R} = 0 \tag{6}$$

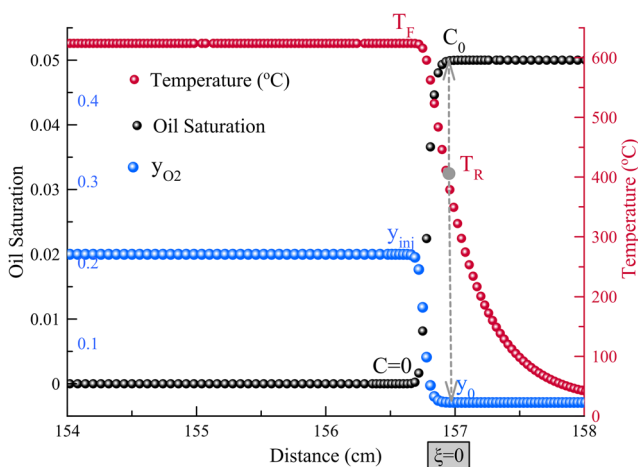


Fig. 9 Profile of temperature (red), oil saturation (black), oxygen composition (blue) in the vicinity of the reaction front

$$\frac{\partial(\dot{m} y)}{\partial \xi} + \sigma A \dot{R} = 0 \tag{7}$$

$$V \frac{\partial C}{\partial \xi} - \frac{\partial C}{\partial \theta} = \dot{R} \tag{8}$$

$$\lambda A \frac{\partial^2 T}{\partial \xi^2} + Q \dot{R} A = \dot{m} c_p \frac{\partial T}{\partial \xi} + A c_s \frac{\partial T}{\partial \theta} - A V c_s \frac{\partial T}{\partial \xi} \tag{9}$$

and Eq. 5 is written as:

$$\lambda A \frac{\partial^2 T}{\partial \xi^2} + Q \dot{R} A = \frac{\partial(mH)}{\partial \xi} + A c_s \frac{\partial T}{\partial \theta} - A V c_s \frac{\partial T}{\partial \xi} \tag{10}$$

At sufficiently large time, the condition is assumed to be steady-state in the vicinity of the reaction front [5]. At steady-state conditions ($\frac{\partial}{\partial \theta} = 0$), Eqs. 6 and 8 are combined and integrated to give:

$$\dot{m} = \dot{m}_{inj} + A V C \tag{11}$$

Similarly, Eqs. 7 and 8 are combined and integrated to give:

$$y = \frac{\dot{m}_{inj} y_{inj} - \sigma A V C}{\dot{m}_{inj} + A V C} \tag{12}$$

Equations 8 and 10 are combined and integrated to give:

$$\lambda A \frac{\partial T}{\partial x} + Q V A (C - C_0) = (\dot{m} c_p - A V c_s)(T - T_i) \tag{13}$$

We see from Fig. 9, at peak temperature ($T = T_F$), $C = 0$ and $\frac{\partial T}{\partial x} = 0$. This allows us to obtain the peak temperature by using Eq.13 as

$$T_F = T_i + \frac{Q A V C_0}{A V c_s - \dot{m}_{inj} c_p} \tag{14}$$

or

$$T_F = T_i + \frac{Q C_0}{c_s \Delta_1} \tag{15}$$

in which

$$\Delta_1 = 1 - \frac{\dot{m}_{inj} c_p}{A V c_s} \tag{16}$$

We also define:

$$\Delta_2 = 1 - \frac{\dot{m}_{out} c_p}{A V c_s} \tag{17}$$

in which, \dot{m}_{out} is the flue gases mass rate at the producer. In a combustion tube experiment, Δ_1 and $\Delta_2 \approx 1$ (see Fig. 10). This is not necessarily correct for all the smoldering processes but suffices for laboratory studies of ISC. Thus, in general, peak temperature depends on Δ_1 parameters (e.g., injection rate). This conclusion is confirmed by the numerical simulation results.

In the asymptotic approach, reaction rate (2) is written as

$$\dot{R} = R_0 y C \Theta(T - T_R) \tag{18}$$

in which Θ is the step-function. It means that when $T < T_R$, there is no reaction ($\dot{R} = 0$) and for $T \geq T_R$, the reaction rate does not depend on the temperature [20]. In

this way, the non-linearity is handled as the discontinuity of the reaction rate. Nevertheless, relevant values of T_R and R_0 must be used. Here is where the Zeldovich concept is applied [20]:

$$T_R = T_F - \frac{R T_F^2}{E} \tag{19}$$

T_R is the temperature at which the reaction starts. As shown in Fig. 9, at $\xi = 0$, we have $T(0) = T_R$, $C(0) = C_0$, and $y(0) = y_0$. When the front propagates, y_0 is always non-zero, even in the filtration regime (when y in the producer (y_{out})=0). Nevertheless, y_0 is a good estimation for y_{out} . Similarly, \dot{m}_0 is the mass rate at $\xi = 0$ and is a good estimation for \dot{m}_{out} . From Eqs. 11 and 12, we find that:

$$\begin{aligned} \dot{m}_0 &= \dot{m}_{inj} + A V C_0 \\ y_0 &= \frac{\dot{m}_{inj} y_{inj} - \sigma A V C_0}{\dot{m}_{inj} + A V C_0} \end{aligned}$$

The Zeldovich number is defined as

$$Ze = \frac{T_R - T_i}{T_F - T_R} \tag{20}$$

and because T_R is in the order of T_F , much bigger than T_i (assuming a highly exothermic reaction), we write:

$$Ze \approx \frac{E}{R T_F}$$

R_0 is obtained either by integration [14] or by the method of [37] to be

$$R_0 = a P e^{(-\frac{E}{R T_F})} \tag{21}$$

T_0 and R_0 are derived for the case of gasless combustion. Nevertheless, numerical experimentation shows that these values give good estimations (see Table 4).

Finding the front velocity (V), is more challenging. Reference [6] used the ZFK approximation of velocity. The ZFK estimation is obtained under assumption of gasless combustion and zero-order of oxygen in the reaction rate. Reference [31] derived estimations for velocity under a smoldering condition. These assumptions [53] result in inaccurate velocity predictions.

In an original approach, we have derived a formula for velocity (See Appendix 7.1). We found that:

$$V = \sqrt{\frac{R_0 \lambda}{c_s} \frac{y_0 \Delta_2}{Ze}} \tag{22}$$

is an accurate estimation of front velocity (Table. 4). It has a form similar to the ZFK velocity except for the coefficient of $y_0 \Delta_2$. Clearly, $y_0 \Delta_2$ depends on the velocity. So velocity is found by solving (22).

Having the front velocity, other parameters listed in Table 4 are calculated. We see from Table 4 that our analytical formulas give a good estimation of results found by the numerical simulation with input shown in Table 1. Now, we are able to define the relevant non-dimensional parameters.

3.3 Non-dimensional form

To analyze the physical stability of the problem, it is useful to find relevant non-dimensional parameters. We define:

$$\begin{aligned} \dot{m} &= \widehat{m} \dot{m}_{inj} \\ Y &= \dot{m} y \\ Y &= \widehat{Y} \dot{m}_{inj} Y_0 \\ C &= \widehat{C} C_0 \\ T &= \widehat{T} (T_F - T_i) \\ \tau &= \widehat{\tau} \theta \\ \xi &= \widehat{\xi} L \end{aligned}$$

The reaction rate is:

$$\dot{R} = a P y C e^{(-\frac{E}{RT})} = a P y_0 C_0 e^{(-\frac{E}{RT_F})} \frac{\widehat{Y} \widehat{C}}{\widehat{m}} e^{(\frac{E}{RT_F} - \frac{E}{RT})}$$

with defining \ddot{R} as

$$\ddot{R} = a P y_0 C_0 e^{(-\frac{E}{RT_F})} \tag{23}$$

we have:

$$\dot{R} = \ddot{R} \frac{\widehat{Y} \widehat{C}}{\widehat{m}} e^{(\frac{E}{RT_F} - \frac{E}{RT})}$$

Table 4 Comparison of analytical solution and numerical simulation results for case 1 and 2

Parameters	Case 1		Case2	
	Numerical simulation	Analytical approach	Numerical simulation	Analytical approach
T_F	448	452	624	647
V	0.58	0.39	2.82	3.02
\dot{m}_{out}	4.39	4.28	8.21	7.54
y_{out}	0.005	0.008	0.027	0.03

Assuming a highly exothermic reaction,

$$\widehat{T}_F = \frac{T_F}{T_F - T_i} \cong 1$$

Considering the Zeldovich number from Eq. 20, we have:

$$\dot{R} = \ddot{R} \frac{\widehat{Y}\widehat{C}}{\widehat{m}} e^{Ze(1-\frac{1}{T})}$$

The mass balance equation becomes

$$\frac{m_{inj}}{L} \frac{\partial \widehat{m}}{\partial \xi} = A \ddot{R} \frac{\widehat{Y}\widehat{C}}{\widehat{m}} e^{Ze(1-\frac{1}{T})}$$

in which L is the characteristic length, defined later. We consider the Damköhler number for our problem to be

$$Da = \frac{A L \ddot{R}}{\dot{m}_{inj}} \quad (24)$$

So the first mass balance equation becomes:

$$\frac{\partial \widehat{m}}{\partial \xi} = Da \frac{\widehat{Y}\widehat{C}}{\widehat{m}} e^{Ze(1-\frac{1}{T})} \quad (25)$$

We define:

$$B = \frac{y_{inj}}{\sigma} \quad (26)$$

B is the air to fuel ratio, if the combustion is complete. Our study refers to both complete and incomplete combustion and so it is not the classical air to fuel ratio. Because $\sigma \approx 1$ [51], B is normally between 0 and 1.

The oxygen mass balance equation is written as

$$\frac{\partial \widehat{Y}}{\partial \xi} = - \frac{Da}{B} \frac{y_0}{y_{inj}} \frac{\widehat{Y}\widehat{C}}{\widehat{m}} e^{Ze(1-\frac{1}{T})}$$

But $\frac{y_0}{y_{inj}}$ is not independent of Da and B. With algebraic calculation, we find that

$$\frac{y_0}{y_{inj}} = \frac{1 - Da B}{Da + 1}$$

so the non-dimensional mass balance equation for the oxygen is

$$\frac{\partial \widehat{Y}}{\partial \xi} = \frac{Da (Da + 1)}{B(Da B - 1)} \frac{\widehat{Y}\widehat{C}}{\widehat{m}} e^{Ze(1-\frac{1}{T})} \quad (27)$$

Considering the mass balance equation for the oil, we choose the characteristic length and time (L and θ) as

$$L = \frac{V C_0}{\ddot{R}}$$

$$\theta = \frac{C_0}{\ddot{R}}$$

Thus, the non-dimensional form of the mass balance equation for the oil component is

$$\frac{\partial \widehat{C}}{\partial \xi} - \frac{\partial \widehat{C}}{\partial \theta} = \frac{\widehat{Y}\widehat{C}}{\widehat{m}} e^{Ze(1-\frac{1}{T})} \quad (28)$$

In Appendix 7.2, we show that the non-dimensional form of the energy balance equation is:

$$\Delta_2 Ze \frac{\partial^2 \widehat{T}}{\partial \xi^2} + \Delta_1 \frac{\widehat{Y}\widehat{C}}{\widehat{m}} e^{Ze(1-\frac{1}{T})} = (\widehat{m} - 1 + \Delta_1 \widehat{m}) \frac{\partial \widehat{T}}{\partial \xi} + \frac{\partial \widehat{T}}{\partial \theta} \quad (29)$$

In general, Δ_1 is related to Δ_2 through the Damköhler number:

$$\frac{1 - \Delta_1}{1 - \Delta_2} = Da + 1$$

Equations 25, 27, 28, and 29 are the non-dimensional form of mass and energy balance equations. Boundary conditions are

$$\widehat{\xi} \rightarrow -\infty \Rightarrow \widehat{m} = 1 \quad (30)$$

$$\widehat{\xi} \rightarrow -\infty \Rightarrow \widehat{Y} = \frac{y_{inj}}{y_{out}} = \frac{Da + 1}{(1 - Da B)} \quad (31)$$

$$\widehat{\xi} \rightarrow +\infty \Rightarrow \widehat{C} = 1 \quad (32)$$

$$\widehat{\xi} \rightarrow +\infty \Rightarrow \widehat{T} = 0 \quad (33)$$

$$\widehat{\xi} \rightarrow -\infty \Rightarrow \frac{\partial \widehat{T}}{\partial \xi} = 0 \quad (34)$$

Thus, four dimensionless parameters (Da , Ze , B , and Δ_1) describe the mass and energy balance equations together with their boundary conditions. So the solution for uniform propagation of the front (\widehat{m} , \widehat{Y} , \widehat{C} , and \widehat{T}) is merely dependent on these four dimensionless parameters. This is also correct for derivatives of these solutions ($\frac{\partial \widehat{m}}{\partial \xi}$, $\frac{\partial \widehat{Y}}{\partial \xi}$, $\frac{\partial \widehat{C}}{\partial \xi}$, $\frac{\partial \widehat{T}}{\partial \xi}$, and $\frac{\partial^2 \widehat{T}}{\partial \xi^2}$). Up to this point, we have shown that the uniform propagation of the front is described by an analytical approximation that is governed by four non-dimensional parameters of (Da , Ze , B , and Δ_1). But as we explain in Section 3.4, the stability equations are more involved. We investigate if these non-dimensional parameters are sufficient to analyze the stability.

3.4 Linear stability analysis

Linear stability analysis is a common method to investigate the solution stability of differential equations [38]. During stability analysis, an infinitesimal perturbation is added to the steady-state solution of the differential equations and the evolution of this perturbation with time is analyzed.

Linear stability analysis is based on the assumption that this perturbation is small, at least initially. So the non-linear differential equations are linearized. Boundary conditions are also linearized. Because all parameters used in this section are non-dimensional, we remove the superscript “~”. Thus, we write our four dependent variables as:

$$\begin{aligned} m &= \bar{m} + \tilde{m} \\ Y &= \bar{Y} + \tilde{Y} \\ C &= \bar{C} + \tilde{C} \\ T &= \bar{T} + \tilde{T} \end{aligned}$$

in which “~” superscript indicates the infinitesimal perturbation. When using analytical approximations for linear stability analysis of combustion processes, it is required to consider the perturbation of the front velocity [51]. Otherwise, non-physical results are obtained. Here, we follow the asymptotic approach of [20] that alternatively considers perturbation in the front position ξ_f . With the exception of temperature, the rest of the parameters are constant ahead of the front. Thus, we only include the energy balance equation ahead of the front in our linearized system of partial differential equations:

$$\frac{\partial \tilde{m}}{\partial \xi} = Da \frac{\bar{Y}\bar{C}}{\bar{m}} \left(\frac{\tilde{Y}}{\bar{Y}} + \frac{\tilde{C}}{\bar{C}} - \frac{\tilde{m}}{\bar{m}} \right) \tag{35}$$

$$\frac{\partial \tilde{Y}}{\partial \xi} = \frac{Da(Da+1)}{B(DaB-1)} \frac{\bar{Y}\bar{C}}{\bar{m}} \left(\frac{\tilde{Y}}{\bar{Y}} + \frac{\tilde{C}}{\bar{C}} - \frac{\tilde{m}}{\bar{m}} \right) \tag{36}$$

$$\frac{\partial \tilde{C}}{\partial \xi} - \frac{\partial \tilde{C}}{\partial \theta} = \frac{\bar{Y}\bar{C}}{\bar{m}} \left(\frac{\tilde{Y}}{\bar{Y}} + \frac{\tilde{C}}{\bar{C}} - \frac{\tilde{m}}{\bar{m}} \right) \tag{37}$$

$$\begin{aligned} \Delta_2 Ze \frac{\partial^2 \tilde{T}}{\partial \xi^2} + \Delta_1 \frac{\bar{Y}\bar{C}}{\bar{m}} \left(\frac{\tilde{Y}}{\bar{Y}} + \frac{\tilde{C}}{\bar{C}} - \frac{\tilde{m}}{\bar{m}} \right) = \\ \tilde{m}(1 + \Delta_1) \frac{\partial T}{\partial \xi} + (\bar{m} - 1 + \Delta_1 \bar{m}) \frac{\partial \tilde{T}}{\partial \xi} + \frac{\partial \tilde{T}}{\partial \theta} \end{aligned} \tag{38}$$

$$\Delta_2 Ze \frac{\partial^2 \tilde{T}^+}{\partial \xi^2} = (\Delta_1 + Da + \Delta_1 Da) \frac{\partial \tilde{T}^+}{\partial \xi} + \frac{\partial \tilde{T}^+}{\partial \theta} \tag{39}$$

in which T^+ is the temperature ahead of the front.

The linearized boundary conditions are:

$$\begin{aligned} \xi_f \frac{\partial \tilde{m}(0, \theta)}{\partial \xi} + \tilde{m}(0, \theta) &= 0 \\ \xi_f \frac{\partial \tilde{Y}(0, \theta)}{\partial \xi} + \tilde{Y}(0, \theta) &= 0 \\ \xi_f \frac{\partial \tilde{C}(0, \theta)}{\partial \xi} + \tilde{C}(0, \theta) &= 0 \\ \xi_f \frac{\partial \tilde{T}(0, \theta)}{\partial \xi} + \tilde{T}(0, \theta) &= 0 \\ \xi_f \frac{\partial \tilde{T}^+(0, \theta)}{\partial \xi} + \tilde{T}^+(0, \theta) &= 0 \\ \xi_f \frac{\partial^2 \tilde{T}(0, \theta)}{\partial \xi^2} + \frac{\partial \tilde{T}(0, \theta)}{\partial \xi} &= 0 \\ \xi_f \frac{\partial^2 \tilde{T}^+(0, \theta)}{\partial \xi^2} + \frac{\partial \tilde{T}^+(0, \theta)}{\partial \xi} &= 0 \end{aligned}$$

The boundary condition of the asymptotic model involves $\widehat{T}^+ = \widehat{T} = \widehat{T}_R$. \widehat{T}_R is written in terms of the Zeldovich number as

$$\widehat{T}_R = 1 - \frac{1}{Ze}$$

Because (35), (36), (37), and (38) do not contain explicit θ terms, the solution is written in normal modes as

$$\begin{aligned} \tilde{m} &= f(\xi) e^{s\theta} \\ \tilde{Y} &= g(\xi) e^{s\theta} \\ \tilde{C} &= h(\xi) e^{s\theta} \\ \tilde{T} &= I(\xi) e^{s\theta} \\ \tilde{T}^+ &= J(\xi) e^{s\theta} \end{aligned}$$

and also the front perturbation is written as:

$$\xi_f = \alpha e^{s\theta}$$

This results in a set of ordinary differential equations of six dependent variables that should be solved. The system is stable if the real part of s is negative. The critical stability limit is when the real part of s is zero.

Because all the stability equations and the boundary conditions are formulated using the four non-dimensional parameters (Da , Ze , B , and Δ_1), we conclude that the stability of the system is also governed by these non-dimensional parameters; however, complete linear stability analysis needs a full analytical solution of the original system. As mentioned earlier, full analytical solution for our problem is not possible. The approximate analytical solution (e.g., [1, 33]) are useful for finding the non-dimensional parameters, but when the approximate solutions are used in

the stability analysis, it results in flawed stability limits (see [20]).

The straight forward choice here is to go back to the robust numerical simulation and investigate the effect of the non-dimensional parameters. In fact, we benefit from the analytical approximate solution to find the non-dimensional parameters that govern the dynamics of the full problem and its stability. Importantly, we use numerical simulation to assess how these parameters affect linear ISC. Our approach is:

- Assume $\Delta_1 \approx 1$. This is valid for normal design of the combustion tube tests [42]. For other cases of smoldering combustion, Δ_1 may need to be added to the stability plane.
- For a given set of parameters mentioned in Table 1, calculate Ze , Da , and B .
- Run the simulation. See if the converged results are oscillatory at early and late time. If it is pulsating at both early and late time, the set of Ze , Da , and B parameters yield an oscillatory solution. If it is not oscillatory, the set yields a uniform propagation result. At the critical limit, the solution is oscillatory at the early time but as the front propagates, oscillations dampen out.
- To move from the stable to the oscillatory region, increase Q and C_s proportionally (Fig. 11). This makes the Zeldovich number constant. Because C_s is increasing, the velocity and, consequently, Damköhler number decreases. The velocity can also be decreased by reducing the frequency factor and thermal conductivity. From Eq. 20, the activation energy and the peak temperature are constant and Ze remains constant.
- Keep all the parameters constant. Reduce the activation energy and repeat the previous steps.

This procedure gives a set of critical points (at a given B) in the Da - Ze plane (Fig. 11). Interestingly, we have observed that the critical points (Fig. 11) for a given B , fit a hyperbolic form:

$$Ze_{cr} = a(1 + b Da_{cr})^{(1/c)}$$

Fig. 10 Values of Δ_1 and Δ_2 for the stability test of Fig. 12

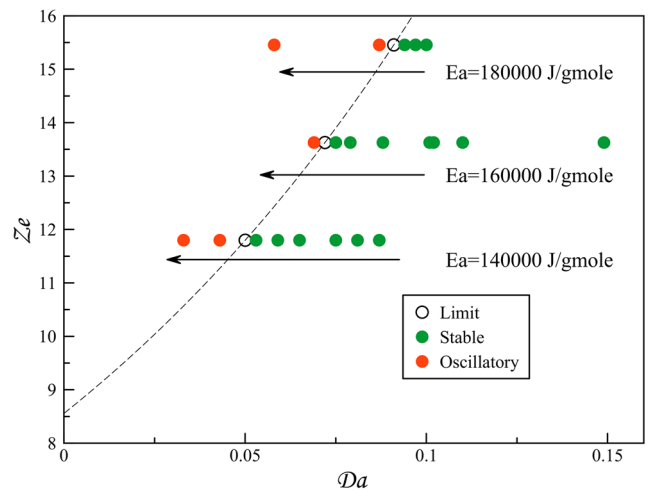
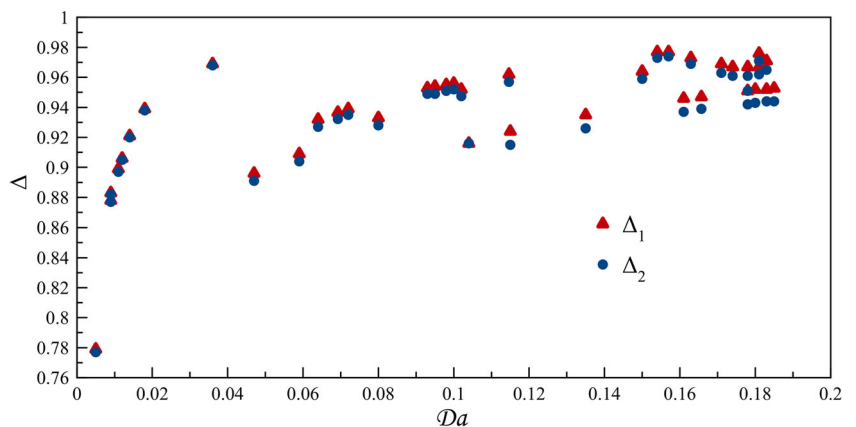


Fig. 11 Procedure to find the stability limit. The parameter B is fixed

We repeat this procedure for different B values. As we mentioned earlier, B is normally between 0 and 1. Here, we have changed B from 0.1 to 0.79 by changing the oxygen composition of the injected gas from 11 to 100 percent. Figure 10 shows the stability limit for different B numbers. The area above the curve is the pulsating region and the area below the curve is the stable region.

Thus, the set of Ze , Da , and B , is able to determine fully the stability of our problem. We have investigated the parameter space (Fig. 12) to see if there is any violation. Figure 12 shows an example of our study for $B = 0.18$. We see that the the stability limit in the $Ze - Da$ plane uniquely determines the stability of different cases, without any exception under the assumption that $\Delta_1 \approx 1$.

Figure 10 shows the value of Δ_1 for different sets of parameters in Fig. 12. Figure 10 verifies the assumption that $\Delta_1 \approx 1$ for normal ranges of parameters. We need to emphasize that our approach is valid for any smoldering combustion process. The stability plane shown in Fig. 13, however, is accurate only when $\Delta_1 \approx 1$.

4 Practical design considerations

To avoid oscillatory ISC, we recommend the following considerations:

1. Injection of air enriched in oxygen [40] helps the propagation of the front, but it causes instability. Larger y_{inj} , increases the front speed. But more importantly, it pushes the stability limit to much larger Damköhler making the design oscillatory.
2. Decreasing the activation energy (and thus, Ze), is a good way to make the propagation faster and more stable. So the use of metal nanoparticles and catalysts [9, 24] improves the stability of front propagation.
3. We have from Eq. 22 that:

$$\frac{Da^2(1 + Da)}{1 - \frac{B}{Da}} \propto \frac{1}{\dot{m}_{inj}^2}$$

and because $\frac{Da^2(1+Da)}{1-\frac{B}{Da}}$ is an increasing function of Da , larger injection rate, yields smaller Da and thus more oscillatory design. Larger injection rate helps the propagation of the front, but it makes the design more oscillatory. This becomes less important when combustion approaches the filtration regime ($Da \approx B$).

4. Larger heat conduction increases the stability. From Eq. 22, larger heat conduction yields larger front velocity and Da . Knowing that $\Delta_1 \approx 1$, heat conduction does not considerably change the peak temperature and thus Ze . So larger heat conduction pushes the combustion into the stable region.

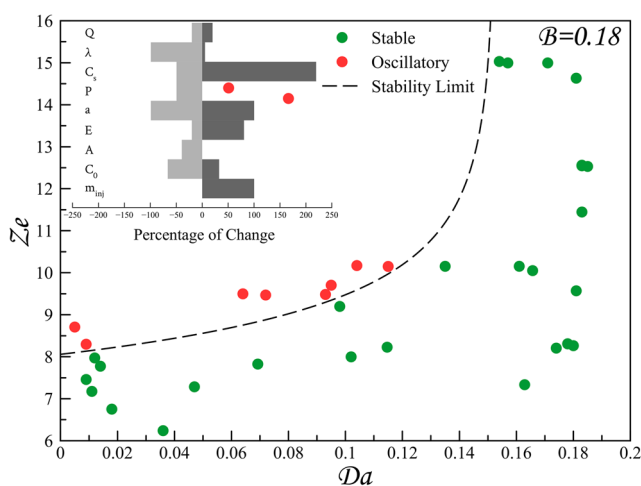


Fig. 12 Stability test for different cases having $B = 0.18$. Solutions to the left of the curve are found to be oscillatory

5. Having more oil in place increases the stability. It increases Damköhler because:

$$\frac{Da^2(1 + Da)}{1 - \frac{B}{Da}} \propto C_0$$

and it decreases Zeldovich by increasing T_f .

6. The effect of heat of reaction on the stability, depends on the parameters. Because

$$\frac{Da^2(1 + Da)}{1 - \frac{B}{Da}} \propto 1/Q$$

larger Q , decreases Da . But larger Q means larger T_f and smaller Ze . Thus, larger heat of reaction may or may not result in more oscillatory design, depending on the condition.

7. To assess the stability of the design:

- **Calculate Da:** estimate front velocity from Eq. 22. Then calculate Damköhler number:

$$Da = \frac{A V C_0}{\dot{m}_{inj}}$$

also calculate Δ_1 to check if $\Delta_1 \approx 1$.

- **Calculate Ze:** activation energy can be estimated from the isconversional approach [16]. Front temperature can be estimated from Eq. 14. Ze is calculated from Eq. 20.
- **Calculate B:** σ is obtained from the kinetics cell experiment [12].

After having the set of (Ze , Da , and B), Fig. 13 is used to assess the stability of the design.

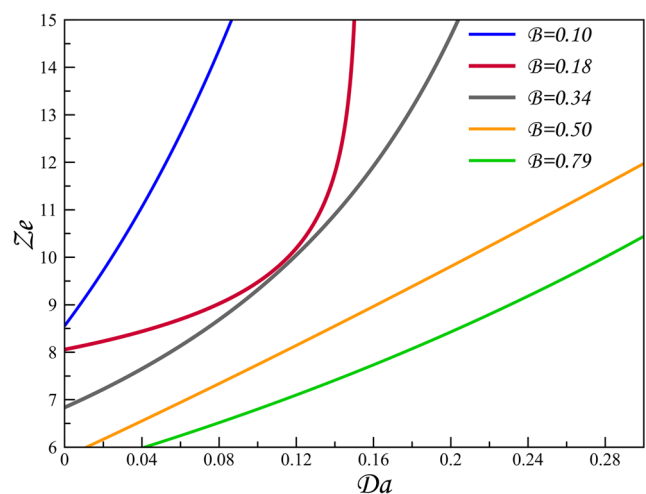


Fig. 13 Stability plane. To the left of a curve for a given B the solution is oscillatory

5 Future work

We have shown that a smaller heat of reaction (larger Ze), drives the system toward the oscillatory region. Heat-loss has a similar effect. Because heat-loss is important to consider in the design of a CT experiment, its effect on stability should be studied. Additionally, a combustion tube experiment is not a perfect one-dimensional ISC. Two-dimensional stability analysis would be beneficial.

In this paper, we have analyzed a simplified CT experiment. In reality, three phases of gas, oil, and water move toward the producer. The effect of transport of different phases on the stability should be included in the analysis. Also, the oxidation kinetics of the crude-oil are complex [10]. In the future we shall investigate the stability of CT tests using more complex kinetics for crude-oil oxidation.

6 Summary

Poor choice of operating conditions for ISC laboratory tests may cause oscillatory propagation of the combustion front. This means that oscillatory behavior of the temperature, flue gas rate, and flue gas composition are observed. Our linear stability analysis suggests that four parameters (Ze , Da , B , Δ_1) govern the stability of the process. Because $\Delta_1 \approx 1$ for laboratory tests, we are able to construct a stability plane based on the set of Ze , Da , B . B is normally between 0 and 1. Larger B , causes more severe oscillations. For a given B , at each Da , there is a critical Ze , at which the system moves from stable to oscillatory conditions by increasing Ze .

Based on our analysis, we found that the best way to achieve stable propagation of the front is to decrease activation energy. Practically, this may be achieved using metal nano-particles and/or metallic salt solutions. Injection of air enriched in oxygen, or larger injection rates, help the front to propagate faster, but the conditions increases the likelihood of oscillations.

Acknowledgements The authors acknowledge Ecopetrol for their help in funding this project. We thank Dr. Franck Monmont for introducing us to the topic of oscillatory ISC. We also thank the members of the SUPRI-A (Stanford University Petroleum Research Institute) Industrial Affiliates.

Appendix

7.1 Front Velocity Calculation

We define the non dimensional parameter

$$\Psi = \frac{\int_{T_x}^{T_F} y C dT}{(T_F - T_x)(y C)_x}$$

By plotting Ψ vs. T (Fig. 14), we observe empirically that at $T = T_R$, $\Psi \approx 1$.

So we have the following

$$\int_{T_R}^{T_F} y C dT = y_0 C_0 (T_F - T_R)$$

From Eq. 8 (with $\frac{\partial}{\partial \theta} = 0$), we have

$$\frac{\partial C}{\partial T} \frac{\partial T}{\partial \xi} V = R_0 y C \Theta (T - T_R)$$

By assuming that $\frac{\partial T}{\partial \xi}$ is constant between T_R and T_F and integration we write:

$$-C_0 \frac{\partial T}{\partial \xi} V = R_0 y_0 C_0 (T_F - T_R)$$

Additionally, from Eq. 13 and knowing that at $\xi = 0$, $C = C_0$, and $T = T_R$, we have:

$$\frac{\partial T}{\partial \xi} = \frac{-(T_R - T_i) V c_s \Delta_2}{\lambda}$$

Hence, we reach (22).

7.2 Non-dimensional Form of the Energy Balance Equation

Starting from the energy balance equation

$$\lambda A \frac{\partial^2 T}{\partial \xi^2} + Q \dot{R} A = \dot{m} c_p - A V c_s \frac{\partial T}{\partial \xi} + A c_s \frac{\partial T}{\partial \theta}$$

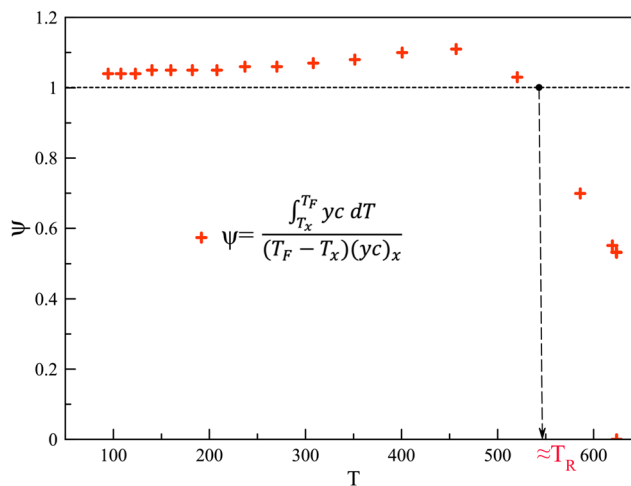


Fig. 14 Ψ vs. T used for front velocity analysis

and using Eq. 22 and dimensionless temperature, we have:

$$\begin{aligned} & \frac{\lambda A(T_f - T_i)}{L^2} \frac{\partial^2 \widehat{T}}{\partial \widehat{\xi}^2} + \\ & (T_F - T_i) \frac{(A V c_s - \dot{m}_{inj})}{V C_0} \ddot{R} \frac{\widehat{Y} C}{\widehat{m}} e^{Ze(1-\frac{1}{r})} \\ & = \left(\frac{\dot{m}_{inj} c_p (T_F - T_i)}{L} \right) \widehat{m} \frac{\partial \widehat{T}}{\partial \widehat{\xi}} - \left(\frac{A V c_s (T_F - T_i)}{L} \right) \frac{\partial \widehat{T}}{\partial \widehat{\xi}} \\ & + \left(\frac{A c_s (T_F - T_i)}{L} \right) \frac{\partial \widehat{T}}{\partial \theta} \end{aligned}$$

Dividing both sides by $T_F - T_i$ and introducing Δ_1 we have:

$$\begin{aligned} & \frac{\lambda A}{L^2} \frac{\partial^2 \widehat{T}}{\partial \widehat{\xi}^2} + \Delta_1 \frac{A c_s}{C_0} \ddot{R} \frac{\widehat{Y} C}{\widehat{m}} e^{Ze(1-\frac{1}{r})} \\ & = -\Delta_1 \left(\frac{A V c_s}{L} \right) \widehat{m} \frac{\partial \widehat{T}}{\partial \widehat{\xi}} + \left(\frac{A V c_s}{L} \right) (\widehat{m} - 1) \frac{\partial \widehat{T}}{\partial \widehat{\xi}} \\ & + \left(\frac{A c_s}{\theta} \right) \frac{\partial \widehat{T}}{\partial \theta} \end{aligned}$$

in which we have added and subtracted the $\widehat{m} \left(\frac{A V c_s}{L} \right) \frac{\partial \widehat{T}}{\partial \widehat{\xi}}$ term. By using Eq. 22, $\frac{\lambda A}{L^2}$ in the first term of the LHS, is written as:

$$\frac{\lambda A}{L^2} = \frac{\lambda A \ddot{R}^2}{V^2 C_0^2} = \frac{A c_s \ddot{R}}{C_0} \left(\frac{T_F}{T_R} \right) Ze \Delta_2 \approx \frac{A c_s \ddot{R}}{C_0} Ze \Delta_2$$

By inserting L and θ in the RHS of the equation, we see that all the terms contain $\frac{A c_s \ddot{R}}{C_0}$. By dividing the equation by $\frac{A c_s \ddot{R}}{C_0}$ and rearranging we reach Eq. 29.

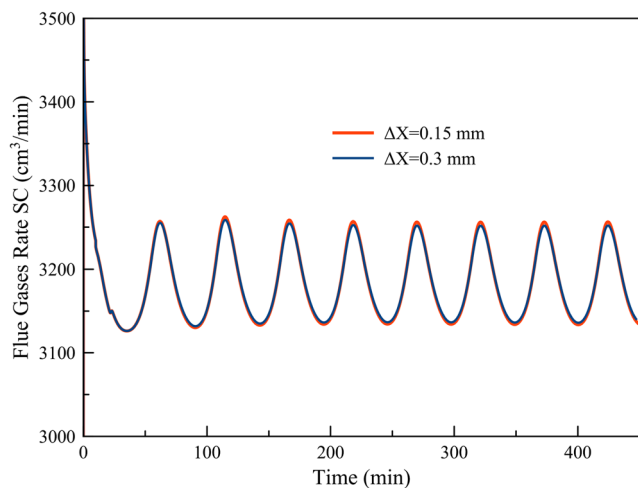


Fig. 15 Flue gases rate for case 1 with $\Delta x = 0.3$ mm and $\Delta x = 0.15$ mm and $\Delta t = 0.01$ min. Note convergence as Δx decreases

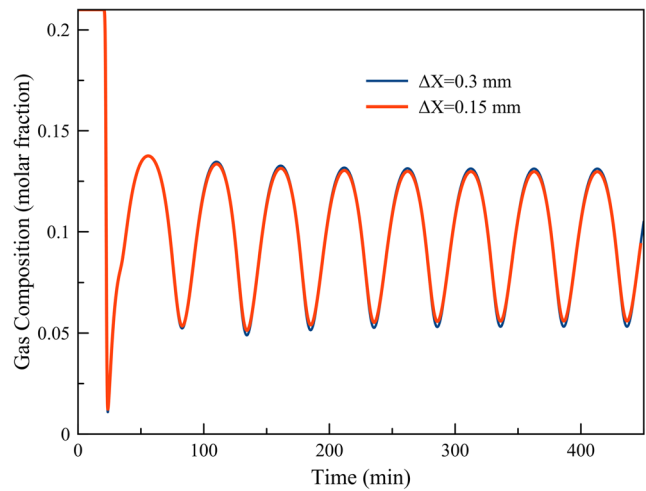


Fig. 16 Oxygen composition in flue gases for case 1 with $\Delta x = 0.3$ mm and $\Delta x = 0.15$ mm and $\Delta t = 0.01$ min. Note convergence as Δx decreases

7.3 Convergence and Stability

We show the convergence of our simulation by temporal and spatial refinement of the simulation. We also show the stability of our numerical simulation to both infinitesimal and finite perturbations.

In general, for $\sigma < 1$, we found that the fully resolved system is achieved by having $\Delta x = 0.3$ mm and $\Delta t = 0.01$ min. Figures 15 and 16 show the flue gas rates and oxygen composition for the case of $\Delta x = 0.3$ mm and $\Delta x = 0.15$ mm. We see that convergence is achieved.

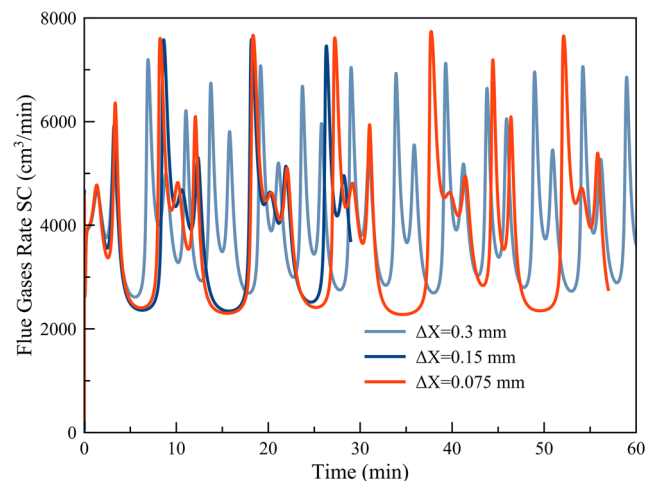


Fig. 17 Flue gases rate for case 2 with $\Delta x = 0.3$ mm, $\Delta x = 0.15$, and $\Delta x = 0.075$ mm and $\Delta t = 0.01$ min. Note convergence as Δx decreases

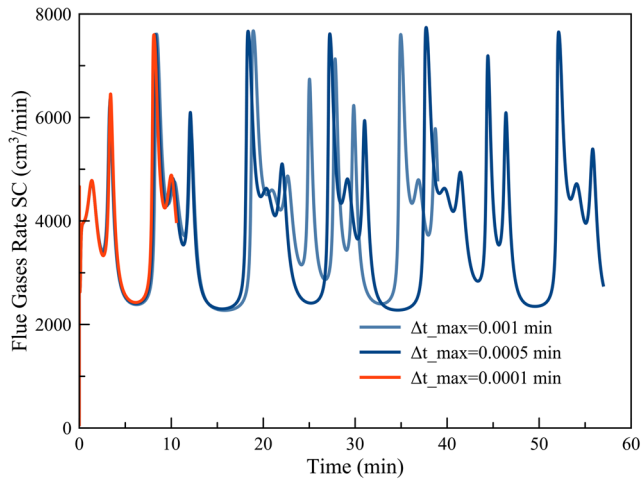


Fig. 18 Flue gases rate of case 2 for $\Delta x = 0.3$ mm with time step sizes of 0.001, 0.0005, and 0.0001 min. Note convergence as Δx decreases

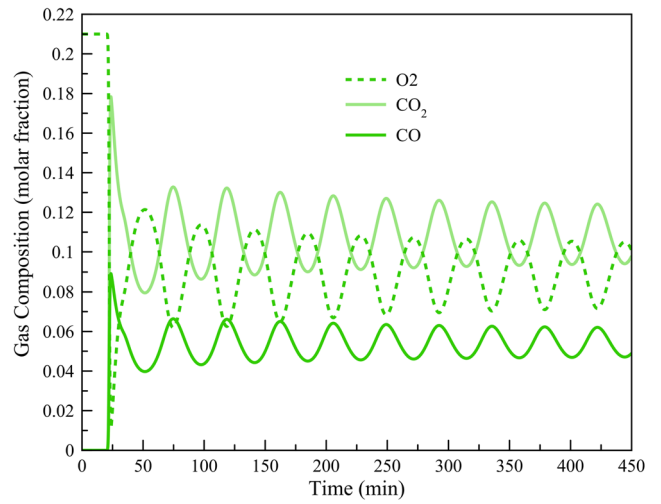


Fig. 21 Flue gases composition profiles for case 1.3

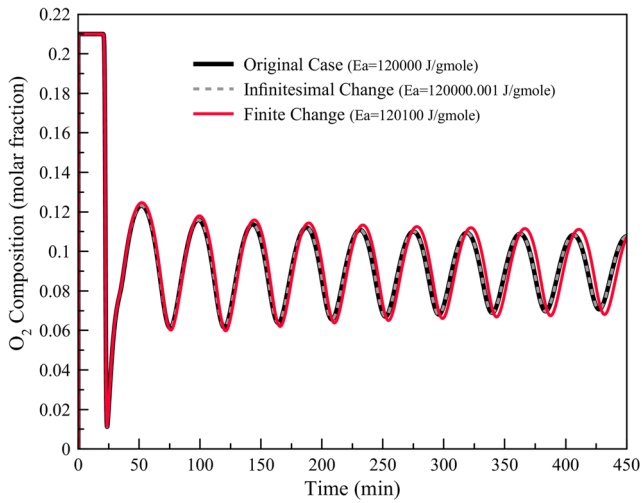


Fig. 19 Stability of numerical simulation (with $E_a = 120000$ J/mol) toward infinitesimal change ($E_a = 120000.001$ J/mol) and finite change $E_a = 120100$ J/mol

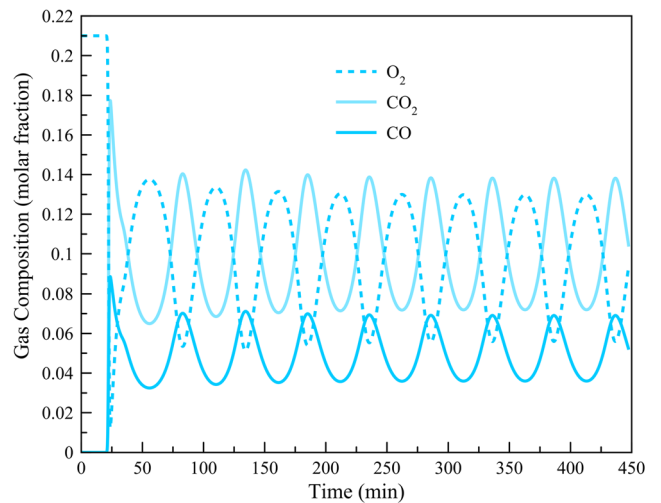


Fig. 22 Flue gases composition profiles for case 1.4

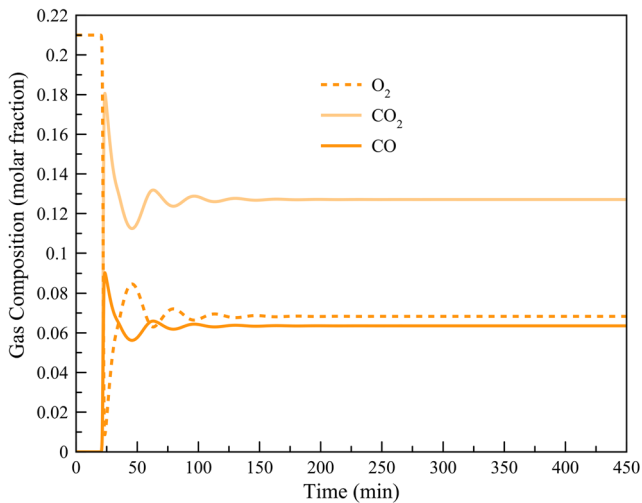


Fig. 20 Flue gases composition profiles for case 1.2

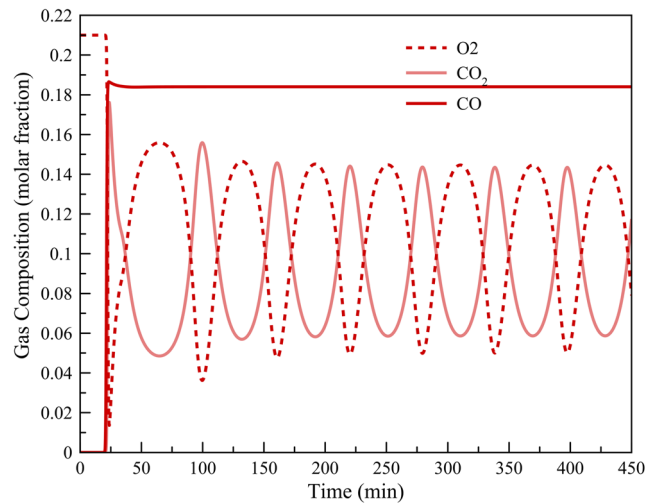


Fig. 23 Flue gases composition profiles for case 1.5

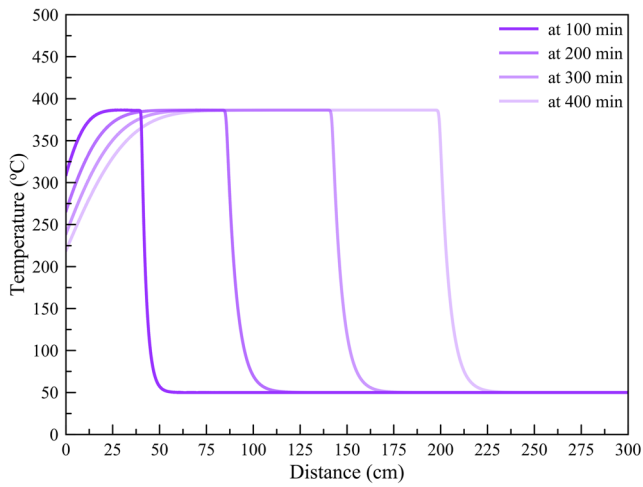


Fig. 24 Temperature profiles at different times for case 1.2

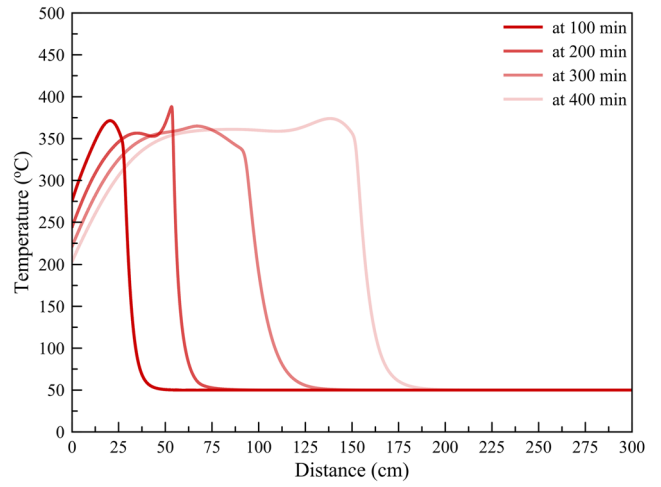


Fig. 27 Temperature profiles at different times for case 1.5

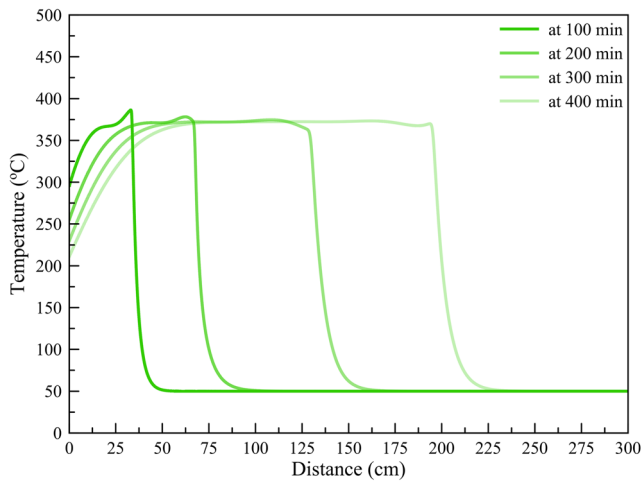


Fig. 25 Temperature profiles at different times for case 1.3

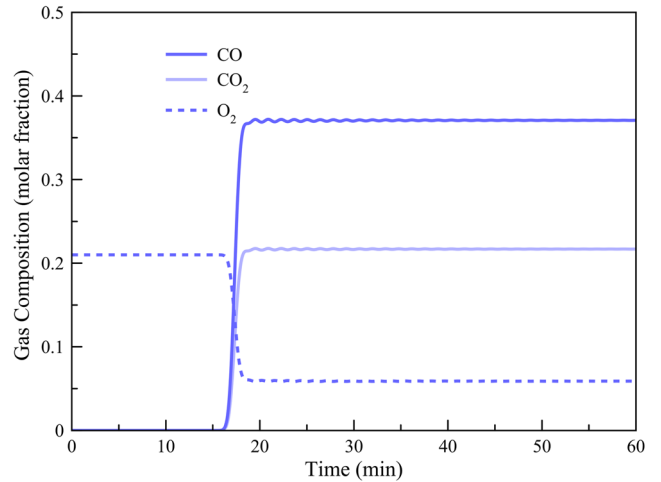


Fig. 28 Flue gases composition profiles for case 2.2

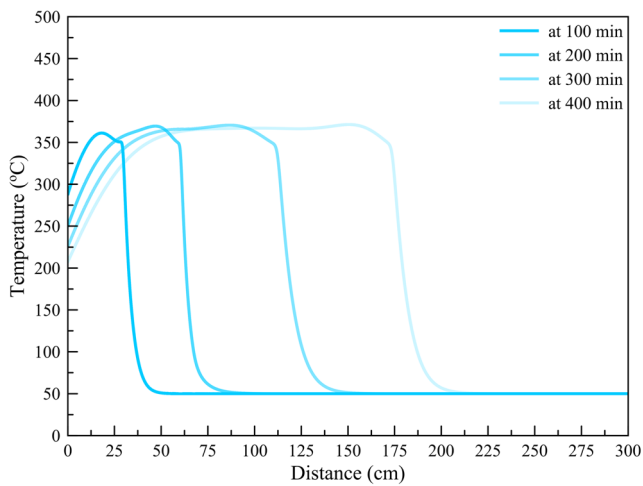


Fig. 26 Temperature profiles at different times for case 1.4

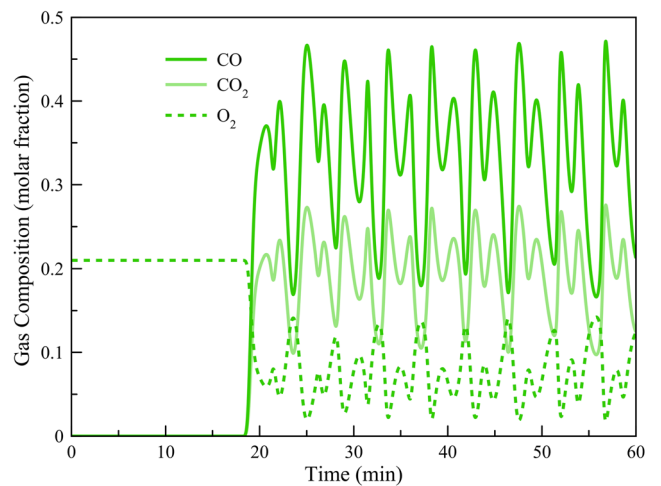


Fig. 29 Flue gases composition profiles for case 2.3

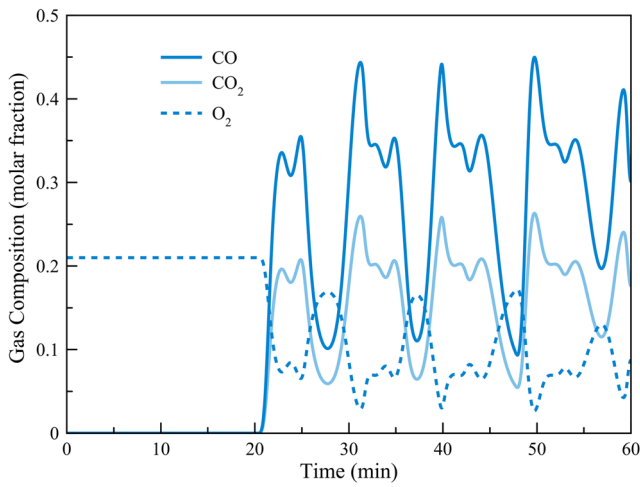


Fig. 30 Flue gases composition profiles for case 2.4

For $\sigma > 1$, we found that the convergence is slower both in temporal and spatial domain. Figure 17 shows the flue gas rate for a time step size of 0.01 min having $\Delta x = 0.3, 0.15,$ and 0.075 mm. Figure 18 shows the flue gas rates for $\Delta x = 0.3$ mm having time step sizes of 0.001, 0.0005, and 0.0001 min.

We also have tested the stability of our numerical simulation against infinitesimal and finite perturbations. The results show that that an infinitesimal change in the parameters does not cause deviation from the original results. Also a finite change in the parameters, causes the results to be in finite difference with the original results. Figure 19 shows the stability of the original numerical simulation (with with $E_a = 120000$ J/mol) toward toward infinitesimal change ($E_a = 120000.001$ J/mol) and finite

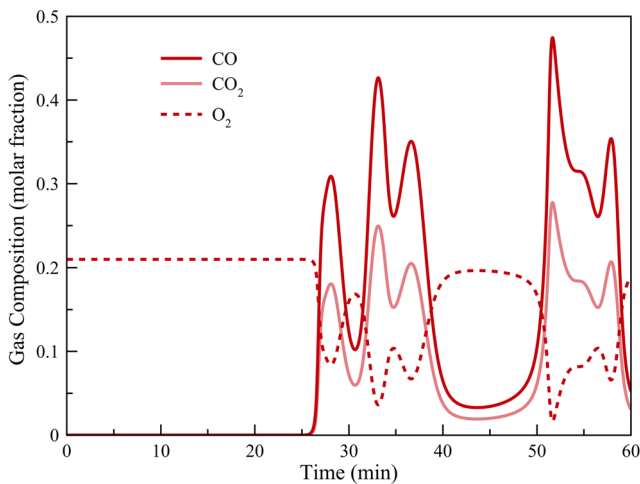


Fig. 31 Flue gases composition profiles for case 2.5

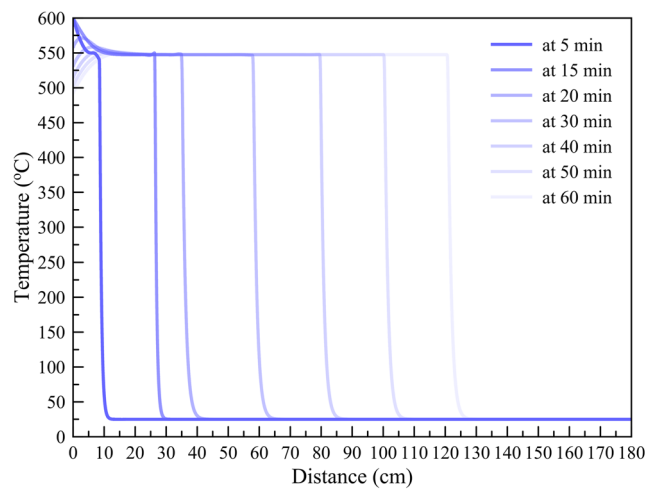


Fig. 32 Temperature profiles at different times for case 2.2

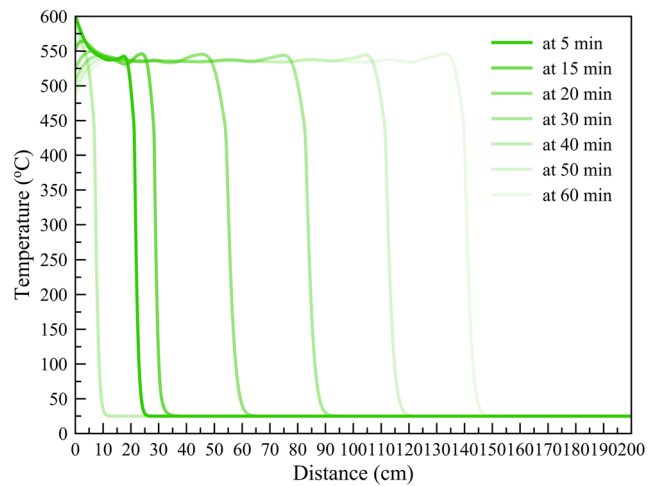


Fig. 33 Temperature profiles at different times for case 2.3

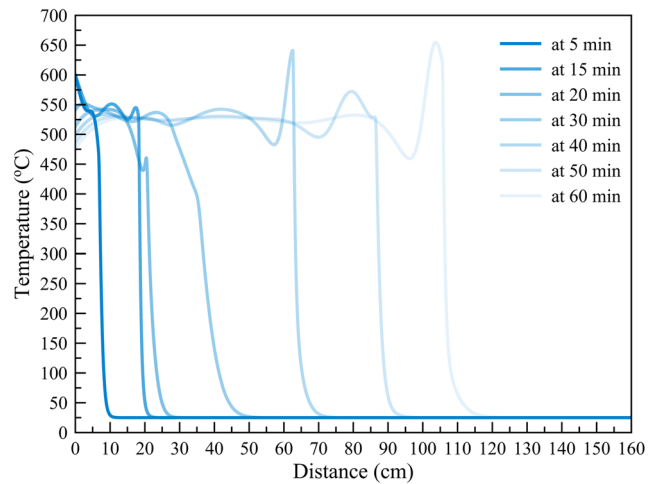


Fig. 34 Temperature profiles at different times for case 2.4

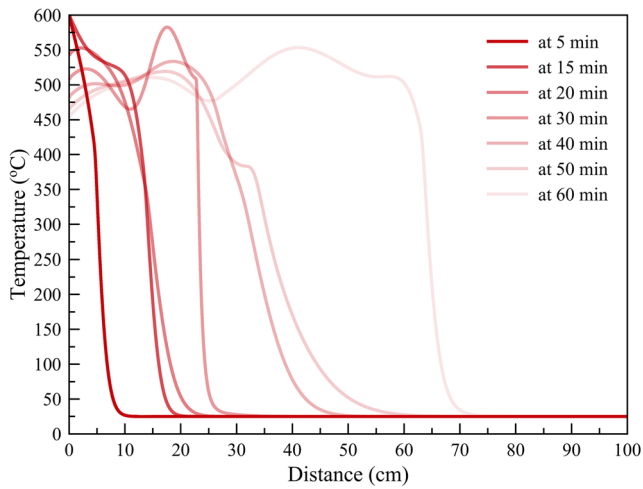


Fig. 35 Temperature profiles at different times for case 2.5

change ($E_a = 120100$ J/mole). As we can see from Fig. 19, the infinitesimal change of activation energy does not change the final result. Also, a finite change in activation energy makes the result to be in finite difference with the original solution.

7.4 Results

It is interesting to see how the oscillation develops with time for different scenarios. Here, we show the results of flue gas compositions, temperature profile, and flue gases rate for cases 1.2, 1.3, 1.4, 1.5, 2.2, 2.3, 2.4, and 2.5 in Figs. 20, 21, 22, 23, 24, 25, 26, 27, 28, 29, 30, 31, 32, 33, and 34.

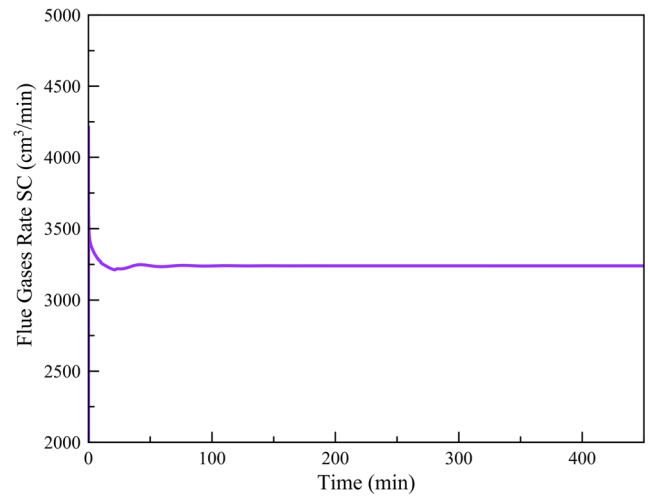


Fig. 37 Flue gases rate for case 1.2

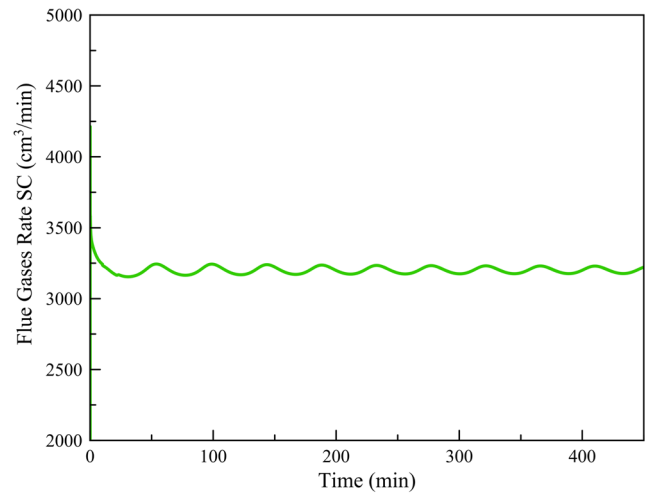


Fig. 38 Flue gases rate for case 1.3

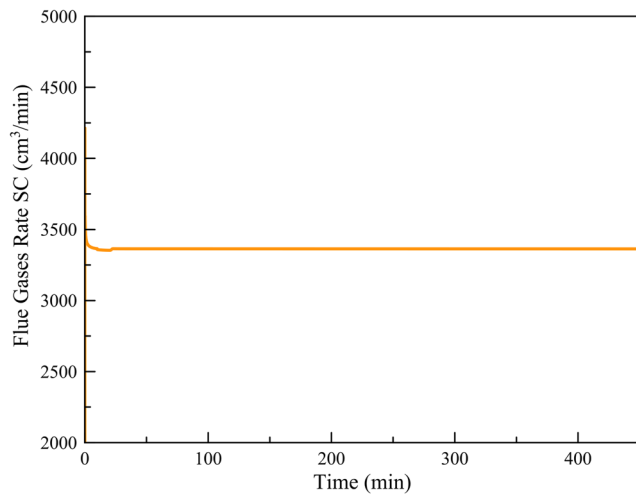


Fig. 36 Flue gases rate for case 1.1

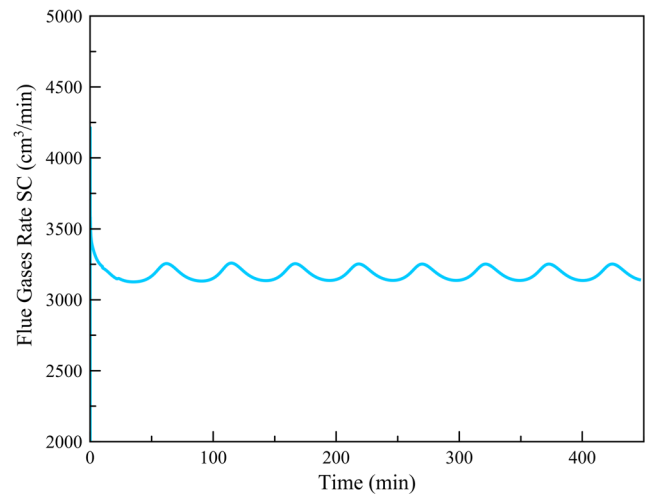


Fig. 39 Flue gases rate for case 1.4

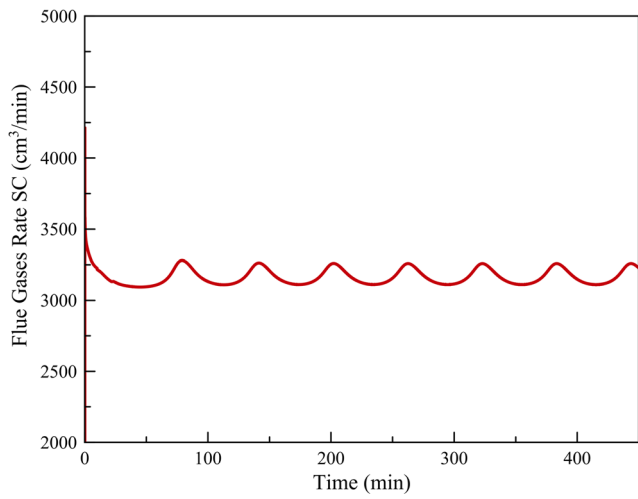


Fig. 40 Flue gases rate for case 1.5

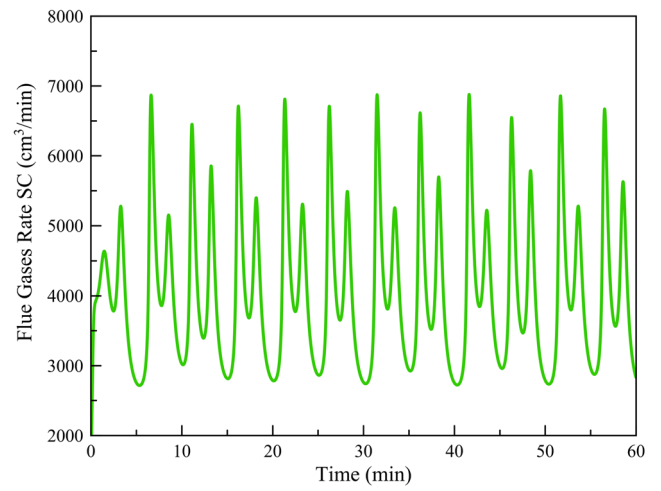


Fig. 43 Flue gases rate for case 2.3

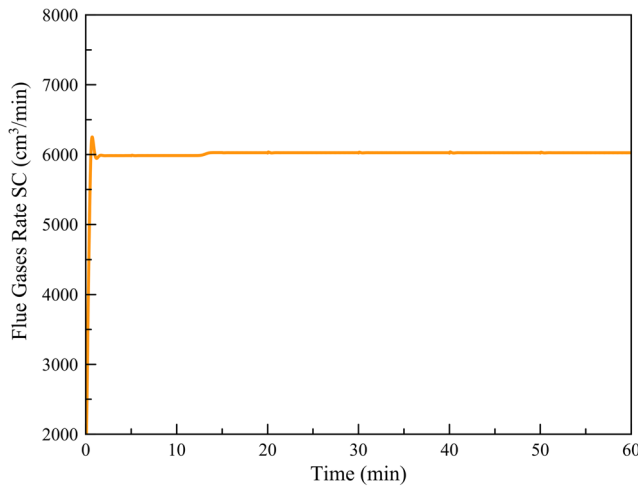


Fig. 41 Flue gases rate for case 2.1

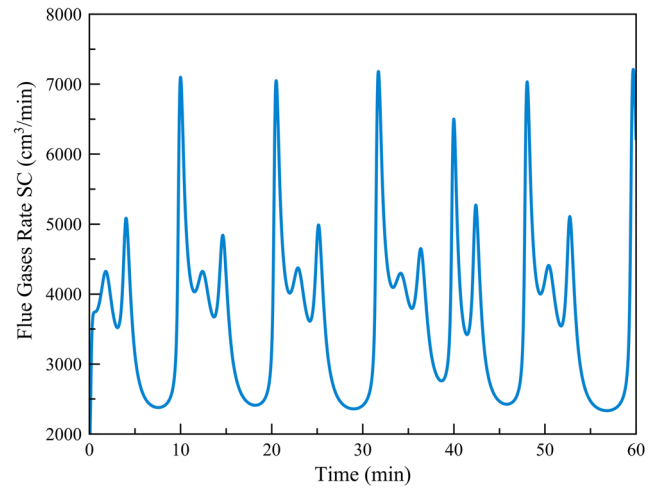


Fig. 44 Flue gases rate for case 2.4

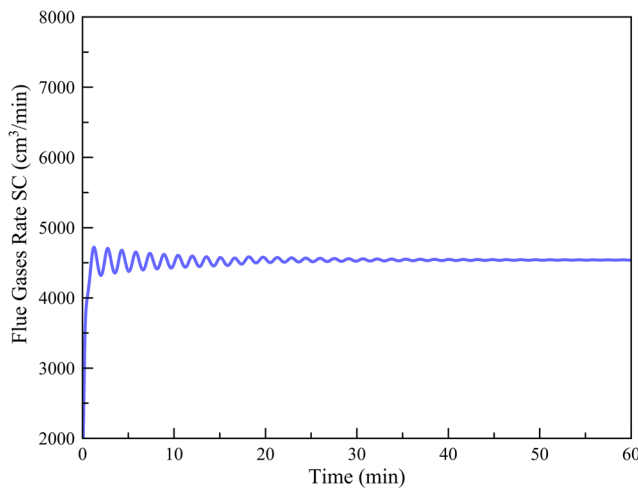


Fig. 42 Flue gases rate for case 2.2

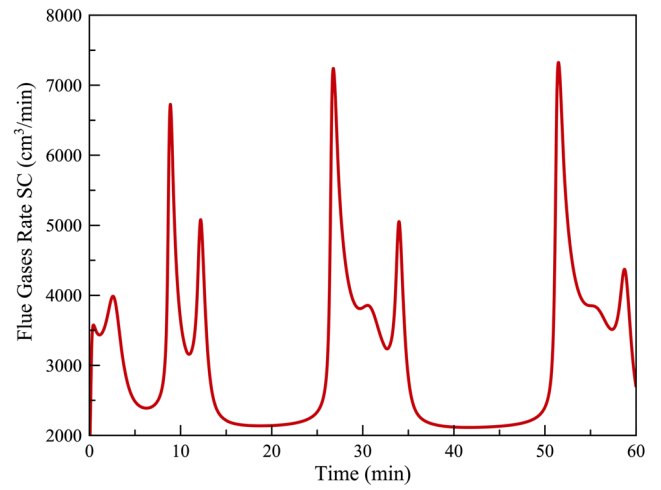


Fig. 45 Flue gases rate for case 2.5

References

- Akkutlu, I.Y., Yortsos, Y.C.: The dynamics of in-situ combustion fronts in porous media. *Combust. Flame* **134**(3), 229–247 (2003)
- Akkutlu, I.Y., Yortsos, Y.C.: The dynamics of in-situ combustion fronts in porous media. *Combust. Flame* **134**(3), 229–247 (2003)
- Akkutlu, I.Y., Yortsos, Y.C., et al.: The dynamics of combustion fronts in porous media. In: SPE Annual Technical Conference and Exhibition, Society of Petroleum Engineers (2000)
- Aldushin, A.: New results in the theory of filtration combustion. *Combust. Flame* **94**(3), 308–320 (1993)
- Aldushin, A.: Filtration combustion. *Advances in combustion science: In honor of Ya B Zel'dovich*(A 97-24531 05-25), Reston, VA, American Institute of Aeronautics and Astronautics, Inc(Progress Astronaut. Aeronaut. **173**, 95–115 (1997)
- Aldushin, A., Kasparyan, S.: Thermodiffusional instability of a combustion front. In: *Soviet Physics Doklady*. vol. 24, p. 29 (1979)
- Aldushin, A., Kasparyan, S.: Stability of stationary filtrational combustion waves. *Combust. Explosion, Shock Waves* **17**(6), 615–625 (1981)
- Aldushin, A., Martem'yanova, T., Merzhanov, A., Khaikin, B., Shkadinskii, K.: Autovibrational propagation of the combustion front in heterogeneous condensed media. *Combust. Explosion, Shock Waves* **9**(5), 531–542 (1973)
- Amanam, U.U., Kovsky, A.R.: Analysis of the effects of copper nanoparticles on in-situ combustion of extra heavy-crude oil. *J. Pet. Sci. Eng.* **152**, 406–415 (2017)
- Bazargan, M., Kovsky, A.R.: A reaction model-free approach for in situ combustion calculations: 1-kinetics prediction. *Transp. Porous Media* **107**(2), 507–525 (2015)
- Bazargan, M., Chen, B., Cinar, M., Glatz, G., Lapene, A., Zhu, Z., Castanier, L., Gerritsen, M., Kovsky, A., et al.: A combined experimental and simulation workflow to improve predictability of in situ combustion. In: SPE Western North American Region Meeting, Society of Petroleum Engineers (2011)
- Bazargan, M., Lapene, A., Chen, B., Castanier, L.M., Kovsky, A.R.: An induction reactor for studying crude-oil oxidation relevant to in situ combustion. *Rev. Sci. Instrum.* **84**(7), 075,115 (2013). <https://doi.org/10.1063/1.4815827>
- Bousaid, I., Ramey, H. Jr., et al.: Oxidation of crude oil in porous media. *Soc. Pet. Eng. J.* **8**(02), 137–148 (1968)
- Buckmaster, J., Clavin, P., Linan, A., Matalon, M., Peters, N., Sivashinsky, G., Williams, F.: Combustion theory and modeling. *Proc. Combust. Inst.* **30**(1), 1–19 (2005)
- Burger, B.C., Sahuquet, J.G.: Chemical Aspects of In-situ Combustion-Heat of Combustion and Kinetics. *SPE Journal* (1972)
- Cinar, M., Castanier, L.M., Kovsky, A.R.: Isoconversional kinetic analysis of the combustion of heavy hydrocarbons. *Energy Fuels* **23**(8), 4003–4015 (2009). <https://doi.org/10.1021/ef900222w>
- Dobrego, K., Zhdanok, S., Zaruba, A.: Experimental and analytical investigation of the gas filtration combustion inclination instability. *Int. J. Heat Mass Transf.* **44**(11), 2127–2136 (2001)
- Firsov, A., Shkadinskii, K.: Combustion of gasless compositions in the presence of heat losses. *Combust. Explosion Shock Waves* **23**(3), 288–294 (1987)
- Ghazaryan, A., Latushkin, Y., Schecter, S., de Souza, A.J.: Stability of gasless combustion fronts in one-dimensional solids. *Arch. Ration. Mech. Anal.* **198**(3), 981–1030 (2010)
- Glazyrin, S., Satorov, P.: Simple model of propagating flame pulsations. *Mon. Not. Royal Astron. Soc.* **416**(3), 2090–2095 (2011)
- Gutierrez, D., Skoreyko, F., Moore, R., Mehta, S., Ursenbach, M., et al.: The challenge of predicting field performance of air injection projects based on laboratory and numerical modelling. *J. Can. Pet. Technol.* **48**(04), 23–33 (2009)
- Hascakir, B., Glatz, G., Castanier, L.M., Kovsky, A., et al.: In-situ combustion dynamics visualized with x-ray computed tomography. *SPE J.* **16**(03), 524–536 (2011)
- Hascakir, B., Ross, C., Castanier, L.M., Kovsky, A., et al.: Fuel formation and conversion during in-situ combustion of crude oil. *SPE J.* **18**(06), 1–217 (2013)
- He, B., Chen, Q., Castanier, L.M., Kovsky, A.R.: Improved in-situ combustion performance with metallic salt additives. In: SPE western regional meeting, Society of Petroleum Engineers (2005)
- Ivleva, T., Merzhanov, A.: Mathematical 3d-modeling for spinning gasless combustion waves. In: *Key Engineering Materials*, Trans Tech Publ. vol. 217, pp. 13–20 (2002)
- Khaikin, B., Merzhanov, A.: Theory of thermal propagation of a chemical reaction front. *Combust. Explosion Shock Waves* **2**(3), 22–27 (1966)
- Kostin, S., Krishenik, P., Shkadinskii, K.: Experimental study of the heterogeneous filtration combustion mode. *Combust. Explosion Shock Waves* **50**(1), 42–50 (2014)
- Kovsky, A., Castanier, L.M., Gerritsen, M., et al.: Improved predictability of in-situ-combustion enhanced oil recovery. *SPE Reserv. Eval. Eng.* **16**(02), 172–182 (2013)
- Kumar, M., et al.: Simulation of laboratory in-situ combustion data and effect of process variations. In: SPE symposium on reservoir simulation, Society of Petroleum Engineers (1987)
- Lebedev, A., Sukhov, G., Yarin, L.: Stability of filtration combustion. *Combust. Explosion Shock Waves* **12**(6), 775–779 (1976)
- Lewis, B., Von Elbe, G.: Theory of flame propagation. *Chem. Rev.* **21**(2), 347–358 (1937)
- Lin, C.Y., Chen, W.H., Lee, S.T., Culham, W.E.: Numerical Simulation of Combustion Tube Experiments and the Associated Kinetics of In-Situ Combustion Processes. *SPE Journal* (1984)
- Mailybaev, A., Bruining, J., Marchesin, D.: Analysis of in situ combustion of oil with pyrolysis and vaporization. *Combust. Flame* **158**(6), 1097–1108 (2011)
- Mailybaev, A.A., Bruining, J., Marchesin, D., et al.: Analytical formulas for in-situ combustion. *SPE J.* **16**(03), 513–523 (2011)
- Makhviladze, G., Novozhilov, B.: Two-dimensional stability of the combustion of condensed systems. *J. Appl. Mech. Techn. Phys.* **12**(5), 676–682 (1971)
- Maksimov, E., Merzhanov, A.: Theory of combustion of condensed substances. *Combust. Explosion Shock Waves* **2**(1), 25–31 (1966)
- Matkowsky, B., Sivashinsky, G.: Propagation of a pulsating reaction front in solid fuel combustion. *SIAM J. Appl. Math.* **35**(3), 465–478 (1978)
- Moin, P.: Fundamentals of engineering numerical analysis. Cambridge University Press, Cambridge (2010)
- Moore, R., Ursenbach, M., Lareshen, C., Mehta, S.: Observation and design considerations for in-situ combustion. Petroleum Society of Canada, Canada (1997)
- Moore, R.G., Bennion, D.W., Belgrave, J.D.M., Gie, D.N., Ursenbach, M.G.: New insights into enriched-air in-situ combustion. *J. Pet. Technol.* **42**(07), 916–923 (1990)
- Panait-Patica, A., Serban, D., Ilie, N., Pavel, L., Barsan, N., et al.: Suplacu de barcau field-a case history of a successful in-situ combustion exploitation. In: SPE Europepec/EAGE Annual Conference and Exhibition, Society of Petroleum Engineers (2006)
- Penberthy, W.L., Ramey, H.J.: Design and operation of laboratory combustion tubes. *Soc. Pet. Eng. J.* **6**(02), 183–198 (1966)

43. Prats, M.: Thermal Recovery. Society of Petroleum Engineers Monograph, p. 7 (1982)
44. Sarathi, P.S.: In-situ combustion handbook—principles and practices, p. 73005. Technical report, National Petroleum Technology Office U.S. Department of Energy, BDM Petroleum Technologies P.O. Box 2565, Bartlesville (1999)
45. Schult, D., Matkowsky, B., Volpert, V., Fernandez-Pello, A.: Forced forward smolder combustion. *Combust. Flame* **104**(1), 1–26 (1996)
46. Schult, D.A.: Matched asymptotic expansions and the closure problem for combustion waves. *SIAM J. Appl. Math.* **60**(1), 136–155 (1999)
47. Shkadinskii, K., Khaikin, B., Merzhanov, A.: Propagation of a pulsating exothermic reaction front in the condensed phase. *Combust. Explosion Shock Waves* **7**(1), 15–22 (1971)
48. STARS: CMG, COMPUTER MODELLING GROUP LTD. 450 Gears Road, Suite 600 Houston, p. 77067, <http://www.cmgl.ca/software/stars2014> (2015)
49. Thomas, F., Moore, R., Bennion, D., et al.: Kinetic parameters for the high-temperature oxidation of in-situ combustion coke. *Journal of Canadian Petroleum Technology* 24(06). <https://doi.org/10.2118/85-06-05> (1985)
50. Wahle, C., Matkowsky, B., Aldushin, A.: Effects of gas-solid nonequilibrium in filtration combustion. *Combust. Sci. Technol.* **175**(8), 1389–1499 (2003)
51. Yarin, L.P., Hetsroni, G., Mosyak, A.: Combustion of two-phase reactive media. Springer Science & Business Media, Berlin (2013)
52. Zeldovich, I., Barenblatt, G.I., Librovich, V., Makhviladze, G.: Mathematical theory of combustion and explosions (1985)
53. Zeldovich, Y.B.: Selected Works of Yakov Borisovich Zeldovich, Volume I: Chemical Physics and Hydrodynamics, vol. 1. Princeton University Press, Princeton (2014)
54. Zhu, Z., Bazargan, M., Lapene, A., Gerritsen, M., Castanier, L., Kovscek, A.: Upscaling for field-scale in-situ combustion simulation. In: Society of Petroleum Engineers, (2011), <https://doi.org/10.2118/144554-MS>